

AFML-TR-71-200

AD743836

**HEAT TRANSFER AND PRESSURE DISTRIBUTIONS  
ON RE-ENTRY NOSE SHAPES  
IN THE VKI LONGSHOT HYPERSONIC TUNNEL**

**BY**

**B. E. RICHARDS**

**S. CULOTTA**

**J. SLECHTEN**

**VON KARMAN INSTITUTE FOR FLUID DYNAMICS  
72 CHAUSSEE DE WATERLOO  
RHODE-SAINT-GENESE  
BELGIUM**

**61052-70-C-003**

**TECHNICAL REPORT AFML-TR-71-200**

**Approved for public release; distribution unlimited.**

Reproduced by  
**NATIONAL TECHNICAL  
INFORMATION SERVICE**  
U S Department of Commerce  
Springfield VA 22151

**AIR FORCE MATERIALS LABORATORY  
WRIGHT-PATTERSON AIR FORCE BASE, OHIO**

22-399

90

# NOTICE

When Government drawings, specifications, or other data are used for any purpose other than in connection with a definitely related Government procurement operation, the United States Government thereby incurs no responsibility nor any obligation whatsoever; and the fact that the government may have formulated, furnished, or in any way supplied the said drawings, specifications, or other data, is not to be regarded by implication or otherwise as in any manner licensing the holder or any other person or corporation, or conveying any rights or permission to manufacture, use, or sell any patented invention that may in any way be related thereto.

ACCESSION FOR		
CFSTI	WHITE SECTION	<input checked="" type="checkbox"/>
DDG	BUFF SECTION	<input checked="" type="checkbox"/>
UNAL	CSB	<input type="checkbox"/>
JUSTIFICATION		
BY		
DISTRIBUTION/AVAILABILITY CODES		
DIST.	AVAIL.	and or SPECIAL
A		

Copies of this report should not be returned unless return is required by security considerations, contractual obligations, or notice on a specific document.

AIR FORCE: 14-3-72/200

UNCLASSIFIED

Security Classification

DOCUMENT CONTROL DATA - R & D		
(Security classification of title, body of abstract and indexing annotation must be entered when the overall report is classified)		
1. ORIGINATING ACTIVITY (Corporate author) von Karman Institute for Fluid Dynamics		2a. REPORT SECURITY CLASSIFICATION none
		2b. GROUP Hypervelocity Dept.
3. REPORT TITLE DISTRIBUTIONS "Heat transfer and pressure on re-entry nose shapes in the V.K.I. Longshot hypersonic tunnel"		
4. DESCRIPTIVE NOTES (Type of report and inclusive dates) Progress Reports No's 1 and 2 - Period ending June 1971		
5. AUTHOR(S) (First name, middle initial, last name) Bryan E. Richards Salvatore Culotta Jozef Slechten		
6. REPORT DATE June 1971	7a. TOTAL NO. OF PAGES 82	7b. NO. OF REFS 17
8a. CONTRACT OR GRANT NO. USAF Contract F61052-70-C-0031	9a. ORIGINATOR'S REPORT NUMBER(S) Progress Reports No's 1 and 2	
b. PROJECT NO. 7381		
c.	9b. OTHER REPORT NO(S) (Any other numbers that may be assigned this report) N.A.	
d.		
10. DISTRIBUTION STATEMENT <del>Available to the public; distribution is unlimited.</del>		
11. SUPPLEMENTARY NOTES N.A.		12. SPONSORING MILITARY ACTIVITY U.S. Air Force
13. ABSTRACT Heat transfer and pressure distributions have been made on five vehicle nose shapes in the VKI Longshot free piston wind tunnel at M=15 and 20. The flow parameters achieved closely simulate aerodynamic re-entry conditions. The models used in the study were a 50°-8° biconic configuration, with sharp- and blunt-nosed versions and a sharp-nosed version with a machined roughness, and a hemisphere configuration with a smooth and a sand-blast rough surface. These configurations resemble the stable shapes of turbulent and laminar ablating nose cones. Preliminary comparisons have been made with the state-of-the-art engineering predictions. Some discussion about the state of the boundary layer is included.		

DD FORM 1, NOV 61 1473

UNCLASSIFIED

Security Classification

Security Classification							
14.	KEY WORDS	LINK A		LINK B		LINK C	
		ROLE	WT	ROLE	WT	ROLE	WT
	HYPERSONIC  REENTRY ABLATION NOSE SHAPES  HEAT TRANSFER  PRESSURE  LAMINAR BOUNDARY LAYER  TRANSITION CRITERIA						

**HEAT TRANSFER AND PRESSURE DISTRIBUTIONS  
ON RE-ENTRY NOSE SHAPES  
IN THE VKI LONGSHOT HYPERSONIC TUNNEL**

*B. E. RICHARDS*

*S. CULOTTA*

*J. SLECHTEN*

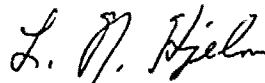
This document has been approved for public release  
and sale; its distribution is unlimited.

## FOREWORD

The activities and results documented in this report were supported under Project 7381 "Materials Application", Task 738102 "Space, Missile and Propulsion System Material and Component Evaluation" with Dr. Merrill L. Minges, Technical Manager for Thermal Protective Systems, Materials Support Division, Air Force Materials Laboratory acting as project engineer. The report covers work conducted during the period May 1970 through July 1971.

The technical advice and guidance of Mr. Victor DiCristina Senior Scientist, Avco Systems Division, Avco Corporation, Wilmington, Massachusetts in the areas of model design and instrumentation, was particularly valuable. Appreciation is also expressed to the Space and Missile Systems Organization (SAMSO) for making several test models available for use on the program.

This technical report has been reviewed and is approved.



L. N. HJEIM, Chief  
Space & Missiles Systems  
Support Branch  
Materials Support Division  
AF Materials Laboratory

## SUMMARY

Heat transfer and pressure distributions have been made on five vehicle nose shapes in the VKI Longshot free piston wind tunnel at  $M=15$  and  $20$ . The flow parameters achieved closely simulate aerodynamic re-entry conditions. The models used in the study were a  $50^\circ$ - $8^\circ$  biconic configuration, with sharp- and blunt-nosed versions and a sharp-nosed version with a machined roughness, and a hemisphere configuration with a smooth and a sand-blast rough surface. These configurations resemble the stable shapes of turbulent and laminar ablating nose cones. Preliminary comparisons have been made with the state-of-the-art engineering predictions. Some discussion about the state of the boundary layer is included.

## LIST OF CONTENTS

### SUMMARY

### LIST OF CONTENTS

### LIST OF FIGURES

### LIST OF TABLES

1. INTRODUCTION	1
2. EXPERIMENTAL APPARATUS	2
2.1 Models	2
2.2 Heat transfer instrumentation	3
2.3 Pressure instrumentation	4
2.4 Measurements of reservoir conditions	6
2.5 Schlieren system	6
2.6 Longshot wind tunnel	7
3. TEST CONDITIONS	8
4. RESULTS	9
4.1 Pointed smooth biconic model (A)	9
4.2 Pointed rough biconic model (B)	11
4.3 Blunt smooth biconic model (C)	12
4.4 Hemisphere models (D,E)	13
5. CONCLUSIONS	15
Acknowledgements	16
References	17
APPENDIX A Data Reduction Programme	A1
APPENDIX B Heat Transfer Data Reduction Programme	B1
APPENDIX C Prediction of Heat Transfer Rate on a Sharp 50° Half-Angle Cone	C1
APPENDIX D Heat Transfer on a Sphere and a Blunt 50° Half-Angle Cone	D1
Tables	
Figures	



## 1. INTRODUCTION

Many investigations of the heat transfer and pressure distributions on re-entry nose shapes have been made in the past. However little experimental data exists on models tested in truly re-entry simulated conditions of high Mach number and high Reynolds number conditions. Measurements of heat transfer on smooth and rough hemispherical and conical bodies will aid predictions of the performance of the ablation method of heat protection. A laminar ablating nose takes on a hemispherical stable shape. In the turbulent case a biconic shape with roughly a  $50^\circ$  forebody with an  $8^\circ$  degree skirt is formed after a long period (Ref. 1).

Some of the outstanding problems necessary to predict ablation recession rates, for instance, are involved with not only verifying the theories used for heat transfer prediction but also knowing the location of the transition of the laminar boundary layer to a turbulent boundary layer on both smooth and rough blunt forebodies.

The current state of the art techniques for predicting laminar heat transfer rates over nose shapes (Ref. 1) involve the use of the laminar stagnation point correlation of Fay and Riddell (Ref. 2) with a local similarity solution (Ref. 3). For turbulent flows then the reference enthalpy method of Eckert (Ref. 4) or Spalding-Chi (Ref. 5) for flat plates is used or a calculation based on the Vaglio-Laurin (Ref. 6) correlation which accounts for pressure gradients.

The models used in experimental study are of two basic types, a hemisphere and a  $50^\circ$ - $8^\circ$  biconic configuration. Both a smooth and an intermediate (sand-blasted) roughness surface was used in the former case. For the biconic shape both sharp- and blunt-nosed smooth models were tested as well as a sharp-nosed version with a very deep waffle-iron-like roughness machined into its forebody. Heat transfer and pressure distributions were

measured on these models in the M=20 flow of the V.K.I. Longshot tunnel. The aerodynamic conditions in this wind tunnel nearly simulate the conditions actually obtained on a re-entering missile during its most critical maximum heating and deceleration phase.

The temperatures at the outside edges of the boundary layers formed on these blunt models are very high, of the order of 2000-2500°K, compared to the wall temperature at ambient conditions. These aerodynamic conditions are beyond those previously compared with the above-mentioned predictions for heat transfer. The gas in the boundary layer is in a vibrationally excited state. Because of the high temperature, the Reynolds numbers on the surface are low, despite the high Reynolds number of the stream. Under such advanced and realistic conditions achieved in these tests, it will be possible to check the ability of the current theories to predict the heat transfer rate on nose cones ablating in a high enthalpy stream.

## 2. EXPERIMENTAL APPARATUS

### 2.1 Models

Five instrumented models fabricated and supplied by AVCO were tested in the Longshot flow. These models were derivatives of two basic shapes, one a biconic and the other a hemispherical model. The biconic model had a 50° half-angled conical forebody of 4 in surface length and an 8° half-angled afterbody leading to a 7 in diameter base. The hemisphere model had a diameter of 7 in.

The biconic shape was tested in three forms. A sharp-nosed model with a smooth wall (called model A in this report), a sharp-nosed model with the forebody roughened with a waffle-iron pattern machined deeply into the surface (B) and a blunt-nosed model (C) with a nose radius of 0.75 in and a smooth surface. The hemisphere was tested in two forms. One a smooth model (D)

and the other a model roughened with a sand-blasted finish (E). Photographs of models B, C, D and E are shown in Fig. 1.

The models were fitted with pressure taps and heat transfer gauges, whose positions are shown in Fig. 2 and listed in Table 1. For each model the meridian containing the pressure taps was at 180 degrees from the meridian containing the heat flux gauges. Because of instrumentation limitations only 10 heat transfer measurements and 7 pressure measurements could be made in one Longshot test.

## 2.2 Heat transfer instrumentation

The flux gauges were fabricated of 0.004 in thick copper disc bonded to an insulating holder as shown in Fig. 3. A chromel-alumel thermocouple junction approximately 0.0015 inches in diameter was formed by spot welding the 0.001 inch diameter thermocouples to the backface of the copper disc. All gauges were contoured to the local body configuration. The discs had a diameter of 0.125 inches except for the rough biconic model (B) which had gauges with disc diameters of 0.110 inches.

Calibration of typical heat flux assemblies were obtained in the ARDC radiant heat flux calibration facility. The purpose of the calibration was to obtain, for a given set of standard material properties, the gauge assembly effective thickness to be used in the heat flux data reduction analysis. Of six gauges tested the average nominal percent deviation is a reduction of 5% in thickness, although the maximum deviation varied from +4.0% to -12.6% in thickness.

For determining the calibration factor of a gauge, the following material properties, supplied by AVCO, of oxygen-free high conductivity copper and chromel-alumel thermocouples were used. The values were averaged over a temperature range from 295°K to 325°K,

Density = 558 lb/ft<sup>3</sup>  
Specific heat = 0.915 B.Th.U/lb/°F  
dT/dV = 44.2°F/mV

Using Equation B.2 (Appendix B) the calibration constant for a calorimeter with a disc of 0.004 inch thick will be  $0.752 \frac{\text{B.Th.U.}}{\text{ft}^2\text{sec}} / \frac{\text{mV}}{\text{sec}}$ . Taking the 5% reduction in thickness into account the calibration constant for a 0.004 inch thick gauge used in the data reduction programme (see Appendix B) was 0.715. Gauges with discs of differing measured thickness were corrected proportionally to that dimension.

Output signals from the calorimeter gauges were generally recorded on Tektronix oscilloscopes using Polaroid cameras. Four channels used some pre-amplification using D.C. amplifiers built at V.K.I. Two channels used in tests on models A and B were recorded on a CEC oscillograph after amplification by CEC D.C. amplifiers. All this instrumentation was calibrated at frequent intervals.

Early tests were carried out in Longshot on gauges with stainless steel calorimeters of 0.001 thickness supplied by AVCO. These tests showed the gauges to be fragile. The heat conduction losses to the thermocouple wires was expected to cause large corrections to the theoretical calibration. These gauges were rejected in favour of copper calorimeters used throughout these tests.

### 2.3 Pressure instrumentation

The pressure taps mounted on the model had internal diameters of        in and channel lengths of        in. The length of rubber tubing of internal diameter        in connecting the pressure taps to the transducer was        in. The internal volume of the total pressure systems was small enough to give a pneumatic response time of less than 1 millisecond.

#### 2.4 Measurements of the reservoir conditions

The reservoir pressure was obtained using a Kistler type 6201 gauge mounted in the wall. The signals were processed and recorded using a Kistler charge amplifier and a Tektronix oscilloscope fitted with a Polaroid camera.

The reservoir temperature was measured with a tungsten-25% rhenium vs. tungsten-3% rhenium thermocouple mounted in the reservoir wall. The wire diameter used was 0.010 in with a total length of approximately 0.5 in giving a response time from 5 to 10 milliseconds. Conduction losses had been assessed in previous tests by using thermocouples with differing  $L/d$  ratios. The method of data reduction is described in Appendix A.

Typical traces from all the above-mentioned instrumentation are shown in Fig. 5.

#### 2.5 Schlieren system

An 18 in conventional, single pass Toepler schlieren system equipped with high quality optical components is used. With the exception of one 24 in plane mirror to bend the light 90° (due to the vicinity of a wall near the test section) the light beam takes a Z shaped path. A single spark light source with a spark duration of 1 microsecond is used to record the visualization of the flow on either a polaroid or a sheet film. The magnification of the system is approximately 0.25. A grid made of nylon line at 1 cm intervals is placed at one of the observation windows. A grid is thus placed on each schlieren photograph. The lines are slightly out of focus, since the schlieren system is focused on the model.

## 2.6 The Longshot wind tunnel

The tests were carried out in the VKI Longshot free-piston wind tunnel (Ref. 7). A photograph of this facility is shown in Fig. 3. Longshot was designed by Pexry and his associates at Republic Aviation specifically for the attainment of very high Reynolds number at high Mach numbers. It differs from a conventional gun tunnel in that a heavy piston is used to compress the nitrogen test gas to very high pressures and temperatures. The test gas is then trapped in a reservoir at peak conditions by the closing of a system of check valves as the piston rebounds. The flow conditions decay monotonically during 10 to 20 milliseconds running time as the nitrogen trapped in the reservoir flows through the nozzle into the pre-evacuated open jet test chamber. The maximum supply conditions currently available are 60,000 psi at 2400°K. Nozzle throat inserts giving nominal Mach numbers of 15 and 20 at the nozzle exit of 14 in diameter were employed in these tests.

The rough-hemisphere model is shown mounted in its test position in the Longshot working section. The shroud mounted around the model is placed to prevent disturbances arising from reflections of the flow from the back wall of the dump tank. The shroud has been proved to be effective in preventing disturbances in the test section occurring before 40 milliseconds after the peak conditions. Such disturbances were mentioned in Ref. 8. The channel sections attached to the shroud lead to the schlieren observation windows. The model is shown mounted on a sting attached to a quadrant traversing system.

### 3. TEST CONDITIONS

The test conditions were computed for each run using the Longshot data reduction programme (outlined in Appendix A). Table 2 summarises the tests carried out in Longshot. Measured reservoir conditions and Pitot pressures at peak conditions are given. Also tabulated are the calculated conditions of Mach number, Reynolds number, dynamic pressure and stagnation point heat transfer on a 7 in diameter hemisphere. Three basic test section conditions were used throughout. These were a high and a low Reynolds number case at  $M=20$ , and a high Reynolds number case at  $M=15$ . The low Reynolds number case, however, was repeated at several slightly differing conditions. This was done since this conditions was tried for the first time during the tests, and it was wished to make sure that the lowest Reynolds number was achieved without condensation occurring.

It is seen that there is reasonable repeatability in the data. Any discrepancies are as much due to the compression cycle (since the pressure developed is very sensitive to the barrel pressure) as the scatter in measurement. The temperature is probably the least accurately measured. Some difficulties occurred with the Pitot probe, since in the  $M=20$  runs, the probe was located very close to the nozzle turbulent boundary layer. In some cases this measurement is suspect.

Fuller details of the test section conditions are given for selected runs for each set of conditions (Table 3). The symbols and units are explained in Appendix A.

#### 4. RESULTS

All measurements of the peak values of heat transfer and pressure are tabulated in Tables 4 to 7 and Tables 8 to 11 respectively. Schlieren photographs of all tests are shown in Fig. 8. The results from each model configuration will be discussed in the following sub-sections.

##### 4.1 Pointed smooth biconic model (A)

Examination of the schlieren photographs of Runs 204 to 210 show that the bow shock remains attached to the nose for all cases. For the zero angle-of-attack cases, the shock wave angle is approximately  $7.5^\circ$  to the surface which agrees to within  $\frac{1^\circ}{2}$  to the theoretical results. This indicates that the flow is supersonic behind the shock.

At the  $\alpha = \pm 10$  cases the shock shape again agrees with the theoretical cone tables of Jones (Ref. 9) to within  $\frac{1^\circ}{2}$ . This is in spite of the fact that the tables have been extrapolated to such an extent that they give subsonic conditions on the windward surface. On the leeward surface, the flow is predicted to remain in a supersonic condition. (It is interesting to note that for  $\theta_c > 20^\circ$ , the shock angle to the surface increases with increasing  $\theta_c$  at these high Mach numbers, a reversal of trend found at low  $\theta_c$ . This is due to the rapid increase of static temperature on the cone surface with increasing  $\theta_c$ .) This means that between the windward surface and the leeward surface, the flow goes from subsonic to supersonic conditions, probably through a sonic line similar to the flow around a yawed cylinder. The luminosity of the flow seen on the windward surface of these bodies is due to slight contaminants in the flow.

Figures 9 to 14 show the reduced pressure data in terms of the pressure coefficient  $c_p = p / \frac{1}{2} \rho V^2$ . Here the dynamic pressure,  $\frac{1}{2} \rho V^2$ , at the nose position is used. The results are shown



compared to the tangent-cone and Newtonian theories in which the corrections outlined in Appendix C are carried out. The value of  $c_p$  for the two theories for a  $50^\circ$  half-angle cone in a parallel flow is given by that value at which the theories cross the  $s=0$  ordinate. The results are seen to agree within a few percent with the tangent-cone theory which itself is roughly 5% above Newtonian theory. Exceptions are seen in Runs 209 and 210 in which the first and third gauges give low values. It is thought that this is caused by non-linear calibration curves (see section 2.3). The results for measurements from 0 to 10 msec after the peak are presented in these figures.

Fig. 15 show the heat transfer rates at peak conditions plotted against local Reynolds number for the zero incidence cases. Three different heat transfer predictions are compared to these results. These are the Eckert reference enthalpy laminar theory, the Sommer and Short reference enthalpy and Spalding-Chi turbulent theories. The formulae used in these predictions are listed in Appendix C. It is seen that all the theories agree reasonably well with the experiments. The trend however is best predicted by the laminar theory. Also the turbulent theories do not compare well with each other. The flow conditions on the surface of the cone as shown in the read out of the program at the end of Appendix C are  $M=1.45$ ,  $T_w=2280^\circ K$  and Reynolds number based on the generator length,  $1.15 \times 10^5$ . The Reynolds number is low essentially because there is a large increase in temperature of the flow over the free-stream condition with only a small change in density. The temperature is high enough that the gas at the edge of the boundary layer is in a vibrationally excited state. Furthermore these conditions are well outside the range of conditions that these engineering theories were correlated. Even though the turbulent theories are as close to the experiment as the laminar theories, since the Reynolds number is low and the trend is better predicted by the Eckert theory, the boundary layer is more likely to be in a laminar state. Further discussion of this topic is given in section 4.3 involved with tests on the blunt cone.

Figs. 16 and 17 show the effect of incidence on the heat transfer rate. The agreement with laminar theory is fair on the "leeward" surface but poor on the windward surface. However as mentioned earlier, the extrapolations of cone tables to these conditions are particularly severe and makes meaningless any attempt at making conclusions.

#### 4.2 Pointed rough biconic model (B)

The heat transfer distributions on the rough model are shown plotted in Figs. 18-20. It is seen that there is a considerable scatter of data along the model. The scattered heat transfer rates and pressure measurements (shown in Fig. 21) obtained with this model indicate that there is appreciable viscous-inviscid interaction of the flow over the sensors, which are buried below the tops of the roughness elements. The low values, for instance, could occur if the sensors are in a separation region. Excluding these low values, the results show a definite trend towards the turbulent boundary layer theories. This is particularly seen in the test at  $M=15$  (Fig. 20) in which the laminar and turbulent theories are more separated.

Several interesting features can be seen from the schlieren pictures of Fig. 8, Runs 211 to 214. In all cases, the bow shock remains attached to the nose. Shock waves emanating from the roughness elements can be seen in the shock region of Run 214. This  $M=15$  case gave higher density levels than the other cases, allowing the gradients to be seen more clearly.

#### 4.3 Blunt smooth biconic model (C)

Fig. 22 shows the reduced pressure data in terms of the pressure coefficient  $c_p$ , for the peak values of each of Run 284 to Run 287. Shown plotted are the theories of Belotserkovskii (Ref. 11) for the spherical nose, and the tangent-cone theory of Appendix C for the cone surface. A dotted line shows the probable pressure variation after the overexpansion region aft of the nose.

It is seen that the pressure recovers from the overexpansion near gauge number 4. The data for the zero incidence case and the leeward surface agree very well with the predictions shown. However, for the windward case, the measurements are somewhat lower than the tangent-cone theory. This could be caused by the high cross-flow on this surface, enhanced by the subsonic flow-field.

Fig. 23 shows the reduced heat transfer data, non-dimensionalised by the measured stagnation point heat transfer predictions for the zero-incidence cases, Run 284 and 287. The results are compared with the laminar similarity theory of Lees (Ref. 3) uncorrected for conicity effects and also the Eckert reference enthalpy method. In these cases, the experiments agree well with these laminar theories. Also the stagnation point heat transfers for these cases agree well with the theory of Fay and Riddell (Ref. 2). This lends support to the supposition that the data on both the blunt and pointed cones are in fact laminar.

The heat transfer data for the yawed cone is shown in Fig. 24 compared with a line drawn through the unyawed cone data of Fig. 23. It is seen that the heat transfer rates for the windward side are much closer to the zero angle of attack results than those measured on the leeward side. This is a similar trend as seen in the pressure distributions of Fig. 22.

The schlieren photographs in Fig. 8 for Runs 284 to 287 show similar effects to that seen in the photographs for the pointed body except in the now detached shock at the nose. Similarly the shock shapes suggest that supersonic flow is found on all surfaces except the windward surface.

#### 4.4 Hemisphere models (D,E)

Figure 25 shows the distribution of pressure non-dimensionalised by an estimated stagnation pressure for all five tests on smooth and rough hemispheres and compared with the theory of Belotserkovskii (Ref. 11) corrected for conicity. It is seen that agreement is excellent. The Pitot pressures have been plotted as the hemisphere stagnation point value. It is seen that these pressures are about 5% higher than suggested by the hemisphere data. These high readings may be explained by the Pitot probe sensing the pressure in the "overshoot" region of the nozzle turbulent boundary layer region as measured in Longshot previously in Ref. 12. This can explain the high degree of scatter obtained in the measurements of Pitot pressure.

The heat transfer measurements for the smooth hemisphere have been compared with the similarity theory of Lees (Ref. 3) corrected for conicity and with a rough correction to align the theory with the pressure curve of Belotserkovskii (Ref. 11) instead of Newtonian theory (Fig. 26). The measurements were non-dimensionalised with respect to the theoretical value of heat transfer rate of Fay and Riddell (Ref. 2). Within 30 degrees of the stagnation point, the measurements are seen to be considerably higher than theory. These results are in disagreement with earlier measurements on a wooden hemisphere model at  $M=15$  reported in Ref. 8 and with the measurements on the stagnation point of model C. A possible reason why the wooden model results gave a different result than in these tests is that the calorimeter gauge was not contoured to the surface. It was assumed at the time that for these large model radii, the disc contouring becomes unimportant. However this discrepancy is puzzling. The differences are too great and are too coincidental to be explained by uncalibrated gauges. These gauges also appeared not to be damaged or eroded during a shot. Possible suggestions are tunnel contaminants or free-stream turbulence, although this does not explain why such

good results were obtained with the 0.75 in radius nose of model C. After  $30^\circ$ , then the results agree very well with the similarity theory of Leet, thus indicating that the flow is laminar.

Fig. 27 shows the results of the rough model displayed in a similar fashion to the smooth model data. Again very high stagnation point heating rates are obtained. High heating rates are seen also generally around the cone, which could be ascribed to either turbulent flow or laminar flow undergoing mixing by the roughness without going turbulent. The highest relative heat transfer rates are found in the  $M=15$  case. This is the most likely case that turbulent flow could be promoted.

The shock stand-off distances from the nose of models C, D and E, as measured from the schlieren pictures of Fig. 8 are shown plotted in Fig. 28 and compared with the theory of Van Dyke as presented in Ref. 19. The comparison is shown to be very good.

## 5. CONCLUSIONS

Tests have been carried out on 3 biconic and 2 hemisphere models in an  $M=15$  and 20 flow in the VKI Longshot. The data has been compared, preliminarily, with simplified theories to assess their quality. The following conclusions can be made from the comparisons.

1. Pressure data on  $50^\circ$  cones and hemispheres agree very well with tangent-cone and the Belotserkovskii theory respectively. An exception was found on the windward side of the  $50^\circ$  blunt cone when lower pressures than expected were found. This was probably caused by cross-flow enhanced by locally subsonic flow behaviour, or due to the severe extrapolation used in the theory.

2. High quality and spatially smooth heat transfer data was obtained on all models except the very rough biconic model. There is some doubt as to whether the cone data is laminar or turbulent due to the similarity in predictions of laminar and turbulent theories at the Longshot flow conditions at  $M=20$ . The evidence weighs more heavily with the presence of laminar flow due mainly to the better prediction in trend of the experimental results by the Eckert reference enthalpy method. Heat transfer measurements on the rough models give good indications that transition to turbulent flows has occurred, especially in the  $M=15$  cases.

3. Stagnation point heat transfer on the blunt cone agreed very well with Fay and Riddell, but some discrepancies have been found with the 7 in hemisphere results.

4. Shock shapes on the conical models and shock stand-off distances from the spherical caps of all the blunt-nosed models agree very well with predictions.

A general conclusion is that useful laminar and turbulent boundary layer heat transfer, pressure and flow visualization data has been achieved on nose shapes in a flow simulating aerodynamic re-entry conditions.

#### ACKNOWLEDGEMENTS

The authors would like to express their thanks to the excellent backing given by the VKI staff : Jean Jugé and Fernand Vandembroeck in the Longshot; Jean-Claude Lobet of the photographic department; and Roger Borrès of the electronics department are specially to be mentioned. The topic originated from and the interpretation of the data was aided by Dr. Merrill Minges of the U.S.A.F. Materials Laboratory and Mr. V. DiCristina of AVCO Corporation, U.S.A.F. Mlle Isabelle Wuilbaut typed the manuscript.

## REFERENCES

1. Minges, M.L. "Ablation Phenomenology" (A review)  
High Temperatures - High Pressures, 1969, Vol. 1,  
pp. 607-649.
2. Fay, J.A., Riddell, F.R., "Theory of stagnation point heat  
transfer in dissociated air", Journal of Aerospace  
Sciences, Vol. 25, 1958, pp. 73-85.
3. Lees, L., "Laminar heat transfer over blunt-nosed bodies  
at hypersonic flight speeds", Jet Propulsion, April,  
1956, pp. 259-269.
4. Eckert, E.R.G., "Engineering relations for skin friction and  
heat transfer to surfaces in high velocity flow",  
Journal of Aerospace Sciences, Vol. 22, p. 585, 1955.
5. Spalding, D.B., Chi, S.W., "The drag of a compressible tur-  
bulent boundary layer on a smooth flat plate with and  
without heat transfer", Journal of Fluid Mechanics,  
Vol. 18, part 1, pp. 117-143, 1964.
6. Vaglio-Laurin, R., "Turbulent heat transfer on blunt-nosed  
bodies in two-dimensional and general three-dimen-  
sional hypersonic flow", J. Aero. Sci., Vol. 27,  
No. 1, January 1960.
7. Richards, B.E., Enkenhus, K.R., "Hypersonic testing in VKI  
Longshot piston tunnel", AIAA Journal, Vol. 8, No. 6,  
June 1970, pp. 1020-1025.
8. Richards, B.E., Enkenhus, K.R., "Stagnation point heat  
transfer and pressure distribution on a hemisphere  
at  $M=15$ ", VKI TR 39, 1970.
9. Jones, D.J., "Tables of inviscid supersonic flow about  
circular cones at incidence  $\alpha=1.4$ ", AGARDograph 137,  
November 1969.
10. Di Cristina, V., "Heat transfer test programme in the VKI  
Longshot hypersonic report", Pre-test Report, AVCO  
Systems Division, AVCO Corporation, April 1971.
11. Hayes, W.D., Probstein, R.F., "Hypersonic flow theory",  
2nd edition, Vol. I, Academic Press, 1966, p. 423.
12. Richards, B.E., Enkenhus, K.R., "The Longshot Free-Piston  
hypersonic tunnel", VKI TN 49, 1968.
13. Enkenhus, K.R., "On the pressure decay rate in the Longshot  
reservoir", VKI TN 40, 1967.



14. Culotta, S., Richards, S.E., "Charts and formulas for determining flow conditions in real nitrogen expanding flows", VKI TN 58, January 1970.
15. Daum, F.L., Gyarmathy, G., "Condensation of air and nitrogen in hypersonic wind tunnels", AIAA J., Vol. 6, No. 3, p. 458-465, March 1968.
16. Slechten, J., "Heat transfer and pressure distribution on a  $5^\circ$  half-angle cone in a conical hypersonic flow", VKI PR 1971.
17. Sommer, S.C., Short, B.J., "Free flight measurements of turbulent boundary layer skin friction in the presence of severe aerodynamic heating at Mach numbers from 2.8 to 7.0", NACA TN 3391, 1955.
18. Wallace, J.E., "Hypersonic turbulent boundary layer studies at cold wall conditions", Proceedings of the 1967 Heat Transfer and Fluid Mechanics Institute, Edited by P.A. Libby, D.B. Olfe, and C.W. Van Atta, June 1967, p. 427-451.
19. Truitt, R.W., "Hypersonic Aerodynamics", The Ronald Press Company, 1959, p. 269.

APPENDIX A

A Short Description of the Longshot  
Data Reduction Programme

A computerised data reduction programme has been devised by Richards, Culotta and Enkenhus and is in general use in Longshot. The details will be written up in a future report. It is appropriate to give a brief description of the method in this report for understanding the results.

In attaining very advanced test conditions, which simulate re-entry flight, the V.K.I. Longshot free-piston wind tunnel displays some unusual features. During a test, dense real nitrogen is trapped in, and allowed to escape from, a constant volume reservoir into a conical nozzle to provide a high Reynolds number, high Mach number test flow. It has been shown theoretically and experimentally (Ref. 13) that the reservoir and test section parameters measured in Longshot can be described accurately by an exponential decay function,  $f$ , of the form :

$$f = \exp (a_0 + a_1 t + a_2 t^2) \quad \text{A.1}$$

where  $t$  is the time in milliseconds from the peak value of  $f$ .

All the measured reservoir and test section pressures and heat transfer rates\* are curve fitted to this formula using a least-squares method (Fig. A.1). The differences between the measured and re-generated values using equation A.1 are found to be within reading error.

The supply temperature is measured with a thermocouple with a long time response\*. Use is made of a formula which connects the temperature explicitly with supply pressure (see Ref. 13)

---

\* Actual traces of reservoir pressure and temperature and Pitot and wall pressures are shown in Fig. 5.

as it decays from a constant volume reservoir to calculate the temperature variation backwards in time from a time when the thermocouple is assessed to be giving the true temperature (Fig. A.2). Conduction losses from the wire and radiation losses from the gas are taken into account to assess the true supply temperature. This difficult temperature measurement will be the object of a further future report by Richards and Enkenhus.

The test gas expands from the reservoir until it becomes a perfect gas in the test section. The density of the gas during the early stages of expansion is high enough that freezing of the internal energy modes does not occur and thus the expansion can be considered as being in equilibrium. A concept of equivalent perfect supply conditions, described in Ref. 1, is used to facilitate the calculation of the test flow parameters,

Supplying the basic recorded oscilloscope or oscillograph deflections and instrumentation calibration data from Longshot's fast response instrumentation, the programme can calculate supply pressure and temperature, Pitot pressure and surface heat transfer and pressure on models. If the two supply conditions and a test section Pitot pressure is supplied, the programme calculates the free stream conditions including Mach number, Reynolds number and dynamic pressure (as described in Ref. 14), the stagnation point heat transfer (Ref. 1 and as in Appendix D) and the test gas condensation temperature (Ref. 15).

A typical set of data obtained in this present series of tests is shown on the next few pages.

The first part of the programme for each measurement gives the calibration constants and the trace deflections, Y divisions (cm or mm) at equal time intervals (as indicated by T) from an easily identifiable position on the trace. Y RAW gives the raw data, Y CORR the smoothed data. Except in the case of the reservoir temperature, the difference between Y RAW and Y CORR is seen to be very small. Comparison of Y RAW and Y CORR under

reservoir temperature illustrates the extrapolation method used. The values agree at the later times in the runs, when the thermocouple has reached its equilibrium temperature, but deviate vastly in the early times showing the slow response of the thermocouple. This difficult measurement is the least accurate of those made in the Longshot, but is considered to be within an error of  $\pm 5\%$ .

The second part of the programme ("quantities measured in Longshot") summarises all the measurements at times from the peak measured conditions using the appropriate curve fit of the actual data to Equation A.1. If a Pitot pressure,  $p_{t_2}$ , is given then for the wall pressures an extra row, YP is given which gives the pressure non-dimensionalized to the dynamic pressure,  $1/2 \rho V^2$ , which is itself approximated using the formula :

$$1/2 \rho V^2 = 0.543 p_{t_2}$$

This formula is true for a perfect gas at hypersonic speeds, but the Pitot pressure measured in Longshot is different from a perfect gas value by about 1% (the actual correction is given in Fig. of Ref. ) due to the gas being vibrationally excited behind the normal shock wave formed ahead of the Pitot probe. Thus YP is approximately 1% lower than the true value. This is well within the limits of the measurements and since it is used only as a rough guide, it has not been thought necessary to make the correction.

The third part of the programme ("Longshot test conditions") reads out at the time intervals from the peak the following variables : measured reservoir pressure, PO (psi); measured reservoir temperature, TO ( $^{\circ}$ K); measured Pitot pressure, PITOT (psi); calculated Mach number; equivalent perfect pressure, POP (psi); equivalent perfect temperature, TOP ( $^{\circ}$ K); Reynolds number per ft; local freestream pressure, P (psi); freestream temperature, T ( $^{\circ}$ K); freestream density, RHO (slugs/ft<sup>3</sup>); stream velocity, V(ft/sec); dynamic pressure, QD (lb/ft<sup>2</sup>); stagnation point

heating on a 7 in diameter spherical surface,  $Q$  (Btu/ft<sup>2</sup>sec); true stagnation temperature,  $TT2R$  (°K); and the temperature at which condensation would occur at that free-stream pressure and expansion rate,  $CONDENSATION$  (°K). These parameters adequately define all the parameters necessary for application to predictive procedures. Care should be taken in that the accuracy of the values printed out should not be inferred from the six significant figures shown. The accuracy is controlled by the accuracy of the measurements inferred in section 2.

# LONGSHOT DATA REDUCTION , RUN 286

NITROGEN DRIVER AND TEST GAS, PISTON WT. = 7.5 LB., P4 = 5000. PSI, P1 = 24.3 PSI.  
DATA PROCESSING, (ZERO TIME DATUM AT POSITION ON TRACE INFLUENCED BY RE-REFLECTED SHOCK)

RESERVOIR PRESSURE  
CALIB. CONSTANTS, GAUGE = 47.62 PSI/MV, SCOPE = 24.6 MV/DIV  
T MSEC 2.0 4.0 6.0 8.0 10.0 12.0 14.0 16.0 18.0 20.0  
Y DIVS. 47.50 42.70 38.80 35.80 33.20 31.20 29.70 28.30 27.00 25.40  
Y RAW 5568.7 50020. 45452. 41937. 38892. 36549. 34792. 33152. 31629. 29754.  
Y CORR. 55168. 50069. 45784. 42180. 39153. 36616. 34502. 32755. 31330. 30193.  
AO = 0.1102E 02 A1 = -0.5411E-01 A2 = 0.9376E-03  
SLOPE -0.05036-0.04661-0.04286-0.03911-0.03536-0.03161-0.02786-0.02411-0.02036-0.01661

RESERVOIR TEMPERATURE  
CALIB. CONSTANTS, SCOPE = 1.163 MV/DIV, HEAT LOSSF = 1.12  
T MSEC 0.0 2.0 4.0 6.0 8.0 10.0 12.0 14.0 16.0 18.0 20.0  
Y DIV 0.00 19.00 23.20 23.80 23.80 23.80 23.60 23.40 23.20 22.80 22.70  
Y RAW 0. 1657. 1962. 2008. 2008. 2008. 1992. 1977. 1962. 1932. 1924.  
Y CORR. 2445. 2361. 2286. 2220. 2161. 2108. 2061. 2020. 1983. 1952. 1924.

## PITOT PRESSURE AT 7.5 DOWNSTREAM OF NOZZLE AND 4.6 FROM CENTRELINE

CALIB. CONSTANT, GAUGE = 0.3040 PSI/MV.  
T MSEC 2.0 4.0 6.0 8.0 10.0 12.0 14.0 15.0 16.0 18.0 20.0  
Y DIVS. 23.80 21.80 20.30 19.00 18.00 16.80 15.70 14.80 14.00 13.10 12.0  
Y RAW 7.43 6.81 6.34 5.93 5.62 5.25 4.90 4.62 4.37 4.09 4.11  
Y CORR. 7.37 6.85 6.39 5.96 5.58 5.23 4.91 4.62 4.35 4.11  
AO = 0.2071E 01 A1 = -0.3760E-01 A2 = 0.2358E-03  
SLOPE -0.03666-0.03371-0.03077-0.02783-0.02488-0.02194-0.01900-0.01605-0.01311-0.01017

## WALL PRESSURE FROM PRESSURE TAP NO. 1

CALIB. CONSTANT, GAUGE = 0.1970 PSI/MV.  
T MSEC 2.0 4.0 6.0 8.0 10.0 12.0 14.0 15.0 16.0 18.0 20.0  
Y DIVS. 19.50 18.00 16.90 15.70 14.40 14.00 13.10 12.50 11.80 11.40 10.0  
Y RAW 3.8415 3.5460 3.3292 3.0928 2.8368 2.7580 2.5806 2.4821 2.3246 2.2458 2.2462  
Y CORR. 3.8391 3.5545 3.3054 3.0873 2.8961 2.7286 2.5821 2.4542 2.3427 2.2462  
AO = 0.1426E 01 A1 = -0.4177E-01 A2 = 0.5454E-03  
SLOPE -0.03959-0.03741-0.03523-0.03305-0.03086-0.02868-0.02650-0.02432-0.02214-0.01995

QUANTITIES MEASURED IN LONGSHOT RUN NO 286  
(ZERO TIME AT PEAK CONDITIONS)

RESERVOIR PRESSURE									
T MSEC	0.0	2.0	4.0	6.0	8.0	10.0	12.0	14.0	16.0
PO PSI	59308.	53544.	48705.	44636.	41215.	38344.	35949.	33941.	32295.
RESERVOIR TEMPERATURE									
T MSEC	0.0	2.0	4.0	6.0	8.0	10.0	12.0	14.0	16.0
TO K	2418.	2338.	2267.	2202.	2145.	2093.	2047.	2007.	1973.
PITOT PRESSURE, PSI, 7.5. FROM NOZZLE EXIT AND 4.6. FROM CENTRE LINE									
T MSEC	0.0	2.0	4.0	6.0	8.0	10.0	12.0	14.0	16.0
Y	7.7640	7.2124	6.7126	6.2592	5.8475	5.4732	5.1325	4.8221	4.5399
YP									18.0
WALL PRESSURE, PSI, GAUGE NO 1									
T MSEC	0.0	2.0	4.0	6.0	8.0	10.0	12.0	14.0	16.0
Y	4.0622	3.7497	3.4763	3.2369	3.0272	2.8435	2.6826	2.5419	2.4191
YP	0.9921	0.9858	0.9820	0.9806	0.9816	0.9851	0.9910	0.9995	1.0105
WALL PRESSURE, PSI, GAUGE NO 2									
T MSEC	0.0	2.0	4.0	6.0	8.0	10.0	12.0	14.0	16.0
Y	2.7719	2.5722	2.3961	2.2407	2.1035	1.9825	1.8756	1.7814	1.6985
YP	0.6770	0.6762	0.6768	0.6788	0.6821	0.6868	0.6929	0.7004	0.7095
WALL PRESSURE, PSI, GAUGE NO 3									
T MSEC	0.0	2.0	4.0	6.0	8.0	10.0	12.0	14.0	16.0
Y	3.2271	2.9775	2.7612	2.5736	2.4110	2.2701	2.1483	2.0434	1.9534
YP	0.7881	0.7828	0.7800	0.7796	0.7818	0.7864	0.7936	0.8035	0.8160
WALL PRESSURE, PSI, GAUGE NO 4									
T MSEC	0.0	2.0	4.0	6.0	8.0	10.0	12.0	14.0	16.0
Y	3.3913	3.1523	2.9420	2.7569	2.5939	2.4504	2.3242	2.2135	2.1166
YP	0.8282	0.8288	0.8311	0.8352	0.8411	0.8489	0.8586	0.8703	0.8841
WALL PRESSURE, PSI, GAUGE NO 5									
T MSEC	0.0	2.0	4.0	6.0	8.0	10.0	12.0	14.0	16.0
Y	3.2427	2.9792	2.7494	2.5488	2.3734	2.2201	2.0860	1.9688	1.8665
YP	0.7920	0.7833	0.7767	0.7721	0.7696	0.7691	0.7706	0.7741	0.7797

LONGSHOT TEST CONDITIONS, RUN NO.286 AT 7.5 IN. FROM NOZZLE EXIT,  
AND 4.6 FROM CENTRELINE

T(MS) MACH NO P(PSI) QD(LB/FT**2)	PO(PSI) POP(PSI) T(K) Q(BTU)	TO(K) TOP(K) RHO TT2R(K)	PITOT(PSI) RE/FT V(FT/SEC) CONDENSATION
0.000 19.946 0.149410E-01 0.599180E 03	0.593082E 05 0.701402E 05 0.387404E 02 0.679880E 02	0.241827E 04 0.312127E 04 0.173726E-04 0.267115E 04	0.776414E 01 0.291117E 07 0.830540E 04 0.356669E 02
2.000 19.786 0.140848E-01 0.555816E 03	0.535447E 05 0.625396E 05 0.376368E 02 0.621384E 02	0.233888E 04 0.298450E 04 0.168572E-04 0.252752E 04	0.721249E 01 0.286180E 07 0.812057E 04 0.354772E 02
4.000 19.653 0.132779E-01 0.516987E 03	0.487051E 05 0.562846E 05 0.366010E 02 0.570995E 02	0.226723E 04 0.286415E 04 0.163412E-04 0.241631E 04	0.571268E 01 0.281271E 07 0.795448E 04 0.352868E 02
6.000 19.548 0.125120E-01 0.481985E 03	0.446367E 05 0.511142E 05 0.356260E 02 0.527424E 02	0.220278E 04 0.275858E 04 0.158201E-04 0.232612E 04	0.625931E 01 0.276314E 07 0.780597E 04 0.350941E 02
8.000 19.472 0.117814E-01 0.450297E 03	0.412161E 05 0.468438E 05 0.346957E 02 0.489543E 02	0.214502E 04 0.266584E 04 0.152957E-04 0.225048E 04	0.584758E 01 0.271408E 07 0.767324E 04 0.348982E 02
9.999 19.427 0.110799E-01 0.421530E 03	0.383440E 05 0.433561E 05 0.337869E 02 0.456433E 02	0.209354E 04 0.258418E 04 0.147719E-04 0.218561E 04	0.547325E 01 0.266766E 07 0.755459E 04 0.346977E 02
12.000 19.408 0.104120E-01 0.395362E 03	0.359409E 05 0.404735E 05 0.329141E 02 0.427462E 02	0.204792E 04 0.251266E 04 0.142496E-04 0.212958E 04	0.513256E 01 0.262216E 07 0.744922E 04 0.344944E 02
14.000 19.415 0.977699E-02 0.371521E 03	0.339418E 05 0.381018E 05 0.320768E 02 0.402118E 02	0.200786E 04 0.245053E 04 0.137297E-04 0.208123E 04	0.482216E 01 0.257739E 07 0.735657E 04 0.342885E 02
16.000 19.448 0.917379E-02 0.349775E 03	0.322954E 05 0.361691E 05 0.312737E 02 0.379965E 02	0.197306E 04 0.239712E 04 0.132135E-04 0.203977E 04	0.453910E 01 0.253328E 07 0.727612E 04 0.340801E 02
17.999 19.506 0.860166E-02 0.329918E 03	0.309603E 05 0.346176E 05 0.305039E 02 0.360637E 02	0.194327E 04 0.235189E 04 0.127020E-04 0.200466E 04	0.428072E 01 0.248973E 07 0.720743E 04 0.338695E 02

H.T. DECAY COEFF..LAM. -0.4748E-01 0.4800E-03

TURB. -0.4995E-01 0.4794E-03 STAG -0.4560E-01 0.5807E-03



## APPENDIX B

### Data Reduction of Calorimetric Heat Transfer Data

As in the previous appendix, this data reduction programme has been perfected in the last few months this time by Culotta and Richards and will again be the subject of a future report.

Calorimeter gauges are constructed of a thin disc of copper bonded to an insulated holder. Thermocouples with a wire diameter smaller than the thickness of the disc are bonded (either welded or soldered) to the back face of the copper disc. The thermocouple senses the average temperature rise of the disc as it heats in the test flow. The heat transfer rate,  $q$ , can then be determined from the following equation :

$$q = k_c \frac{dV}{dt} \quad \text{B.1}$$

where  $k_c$  is the gauge calibration constant

$dV/dt$  is the slope of the thermocouple output variation with respect to time.

The calibration constant,  $k_c$ , is best determined experimentally using a rapidly applied and calibrated heat source. However, it can be calculated from knowledge of the calorimeter thickness ( $b$ ), the density ( $\rho_d$ ) and specific heat, ( $c_d$ ) of the disc material and the thermocouple response parameter  $dT/dV$ , using the following equation :

$$k_c = b \rho_d c_d \frac{dT}{dV} \quad \text{B.2}$$

It must be assumed however that there are no heat conduction losses to the holder or to the thermocouple, the disc thickness is not changed by the welding or soldering of the thermocouple, the temperature is uniform over the volume of the disc.

The order of magnitude of the time constant,  $\tau$ , for the calorimeter may be assessed from :

$$\tau = \frac{\rho_d c_d b^2}{2\kappa}$$

B.3

where  $\kappa$  is the thermal conductivity.

For the testing of a model at rest in a steady flow, equation B.1, is simple to apply for calculating the heat transfer rate from the raw thermocouple output data. The heat transfer rate would be expected to be constant and thus the output will vary linearly with time. It is a simple matter to make a linear least error fit to the data points to achieve the measurement. The method depends upon an assumed knowledge of the variation (but not the level) of the heat transfer with time. In this case it remains constant.

For varying flow conditions alternative methods must be found. More usual methods are to make a polynomial curve fit to the raw data and then to differentiate the formula thus obtained. Often poor results are obtained. If a large order polynomial is chosen although an accurate curve fit to the data is achieved, the derivative can fluctuate wildly about its true variation due to very small errors in reading the data. If a small order polynomial is chosen to eliminate these effects, there is a risk of losing important detail. In general, differentiating a polynomial curve fit to data is usually unsatisfactory.

A new data reduction technique has been devised which uses an extra piece of information to allow the reverse, but more accurate process of the integration of equation B.1. The extra information is the knowledge of the variation (but again not the level) of the heat transfer rate, given in the form of Equation A.1, calculated from the calibrated test section from the Longshot data reduction programme (Appendix A). Three engineering calculations of the heat transfer rate (i.e. the laminar and turbulent heat transfer rate at a fixed position on a flat plate and

the stagnation point heating rate on a sphere) are made in this latter programme, and the coefficients  $a_1$  and  $a_2$  of equation B.1 are determined. These are read out at the very end of the programme as shown in Appendix A. Trial values of the heat transfer at zero time ( $q_{t=0} = f_{t=0} = c^{a_0}$ ) are made and equation B.1 is integrated with this complete information for  $q$ . The calculated transient temperature variation thus obtained is compared with the measured thermocouple output. The value of  $q_{(t=0)}$  that provides the best comparison of the temperature variations is considered the correct value. The remainder of the variation of  $q$  with time is then calculated and read out. The numerical integration is carried out using a Runge-Kutta-Gill-Simpson routine and the search procedure used converges very rapidly.

The above technique is analogous to the method described above for dealing with constant heat transfer data. To summarise, in both methods an assumption is made about the variation (but not the level) of the required parameter, in this case the heat transfer rate. There is no reason why this method cannot be extended to data achieved from more complicated unsteady test section conditions than in Longshot when an appropriate equation, analogous to equation A.1, must be used to describe the heat transfer variation.

To illustrate the technique a typical output from the computer is shown later. A.1 and A.2 are the coefficients defining the slope and curvature data as read from the last line in the Longshot data reduction programme for the appropriate case (i.e. stagnation, laminar, turbulent heat transfer case). K1 and K2 are the oscilloscope calibration in mV/cm or mV/mm and the gauge calibration in  $\frac{\text{B.Th.U.}}{\text{ft}^2\text{sec}} / \frac{\text{mV}}{\text{sec}}$ . Q0 is the value of heat transfer rate in B.Th.U./ft<sup>2</sup>sec at zero time at each iteration step until convergence is obtained. (It is seen that convergence is reached almost immediately). Q(T1) is the final value of heat transfer rate at zero time (peak value). T is the time from peak conditions in msec. Y EXP is the measured oscilloscope deflection (cm or mm). Y CALC is the equivalent calculated value with the

- B 4 -

best fit to the measured data as outlined above. ERR is the difference between Y EXP and Y CALC. (This value is generally within reading errors as can be seen in the example). Q is the heat transfer rate (B.Th.U./ft<sup>2</sup>sec) at time T. For Q(T1) then since the calculation starts at T = 0, then ERR = 0.

DATA REDUCTION OF CALORIMETER HEAT TRANSFER GAUGES, RUN 286, GAUGE 0

A1=-0.49980E-01 A2= 0.48050E-03 K1= 0.10100E 00 K2= 0.73200E 00

Q0= 0.149792E 03

Q0= 0.149792E 03

CONVERGENCE

Q(T1) = 0.14979E 03

T	Y EXP	Y CALC	ERR	Q
2.000	0.52000E 01	0.52586E 01	0.58643E-01	0.13580E 03
4.000	0.91000E 01	0.87635E 01	-0.33643E 00	0.12359E 03
6.000	0.12000E 02	0.11959E 02	-0.40557E-01	0.11291E 03
8.000	0.14900E 02	0.14884E 02	-0.15230E-01	0.10355E 03
10.000	0.17500E 02	0.17572E 02	0.72757E-01	0.95345E 02
12.000	0.20000E 02	0.20052E 02	0.52177E-01	0.88118E 02

## APPENDIX C

### Prediction of Heat Transfer Rate on a Sharp 50° Half-Angle Cone

A computer programme was written by Richards and Slachten to estimate the laminar and turbulent flow over a 50° half-angle cone in a hypersonic conical flow. The equations used are described below.

#### 1. Calculation of the test section conditions

The initial data of the equivalent perfect supply conditions  $(T_0)_{\text{perf}}$  and  $(D_0)_{\text{perf}}$  and the Mach number at an arbitrary, but known position, in the tunnel are supplied as basic input data to the programme. These values are obtained from the Longshot data reduction programme.

The test section conditions can then be obtained using the perfect gas relations :

$$T_1 = T_0(1 + M^2/5)^{-1} \quad (^\circ\text{K}) \quad \text{C.1}$$

$$P_1 = P_0(1 + M^2/5)^{-7/2} \quad (\text{lb/in}^2) \quad \text{C.2}$$

$$\rho_1 = \frac{P_1}{RT_1} \quad (\text{slug/ft}^3) \quad \text{C.3}$$

$$a_1 = \sqrt{\gamma RT_1} \quad (\text{ft/sec}) \quad \text{C.4}$$

$$u_1 = Ma_1 \quad (\text{ft/sec}) \quad \text{C.5}$$

$$\mu_1 = \frac{93.527 T_1^{3/2}}{T_1 + 102.7} \times 10^{-8} \quad \left(\frac{\text{lb}}{\text{ftsec}}\right) \quad \text{C.6}$$

$$Re_1 = \frac{\rho_1 u_1}{\mu_1} \quad (\text{ft}^{-1}) \quad \text{C.7}$$

## 2. Calculation of inviscid flow over a cone

The cone tables of Jones (Ref. 9) for  $\gamma=1.4$  were used to determine the conditions on a cone. For various angles of attack, the tables give the parameters :

$$\frac{u_c}{a_1}, \frac{a_c}{a_1}, \frac{\rho_c}{\rho_1}, \frac{p_c}{\frac{1}{2} \rho_1 u_1^2 \sin^2 \theta_c}, \frac{\theta_s}{\theta_c}$$

as functions of  $M$  and  $\theta_c$ . Here the subscript  $c$  denotes the conditions on the cone surface and subscript  $s$  the conditions at the shock. The range of applicability of Ref. is  $1.5 < M < 20$  and  $5^\circ < \theta_c < 40^\circ$ . This means that for the model under test, extrapolations had to be made from  $\theta_c = 40^\circ$  to  $50^\circ$ .

The tabulated values of the parameters listed above were fitted to a quadratic power series with  $M$  and  $\theta_c$  as the independent variables. The power series was :

$$f = A_1 + A_2 \theta_c + A_3 \theta_c^2 + (A_4 + A_5 \theta_c + A_6 \theta_c^2) M + (A_7 + A_8 \theta_c + A_9 \theta_c^2) M^2 \quad C.8$$

The coefficients  $A_1 \dots A_9$  were obtained by initially fitting quadratics to three sets of data in one of the independent variables. The latter coefficients thus obtained were then cross fitted to quadratics in the other independent variable to obtain the final values of the coefficients,  $A_1 \dots A_9$ . The technique is in effect a two-dimensional interpolation procedure.

Three subroutines were made each for the case of  $\alpha=0$  and  $\alpha=\pm 10^\circ$  (called SLE1, SLE2 and SLE3 respectively).

The pressure on the cone as calculated in this fashion gives the tangent cone value. The modified Newtonian value of pressure is given by  $\rho_1 u_1^2 \sin^2(\theta + \alpha)$ .

### 3. Calculation of conicity effects

Two primary corrections are necessary to account for conicity. One is based on one-dimensional flow considerations, the other on two-dimensional flow considerations.

Regarding the first correction, consider a hypersonic, conical, perfect gas flow. The energy equation for this flow is :

$$h_0 = c_p T_1 + u_1^2/2 \quad \text{C.9}$$

where  $h_0$  is the reservoir enthalpy and  $c_p$  is the specific heat at constant pressure.

For hypersonic flow  $C_p T_1$  is very small compared to  $h_0$ , and thus  $u_1$  becomes nearly constant. Most of the internal energy has been converted to kinetic energy, and the change in Mach number comes mainly from a change in  $T_1$ , hence a change in  $a_1$ .

The continuity equation ( $\rho_1 U_1 A = \text{constant}$ , where  $A$  is a stream tube area) then gives an expression for the density variation,  $\rho$ , at any streamwise position,  $x$ , in a conical flow field :

$$\frac{\rho}{\rho_1} = \sigma^{-1} \quad \text{C.10}$$

$$\text{where } \sigma = \frac{A}{A_1} = \left(1 + \frac{x}{L_n}\right)^2 \quad \text{C.11}$$

here subscript 1 refers to conditions at a reference position,  $L_n$  is the distance from the source point to this position.

Assuming an isentropic expansion :  $p/p_1 = \sigma^{-\gamma}$

$$\text{Equation of state : } T/T_1 = \sigma^{1-\gamma} \quad \text{C.12}$$

$$\text{Sound speed : } a/a_1 = \sigma^{\frac{1-\gamma}{2}} \quad \text{C.13}$$

$$\text{Mach number : } M/M_1 = \sigma^{\frac{\gamma-1}{2}} \quad \text{C.14}$$

Equations C.10 to C.14 can then be used to calculate the stream conditions at any longitudinal position in the expanding flow, knowing the conditions at another position. Refs. and have shown that the Longshot flow in the nozzle is truly conical with its source point located at the nozzle throat.

The second correction factor to account for conicity arises since the flow angle changes by an angle,  $\Delta\alpha = \tan^{-1} \frac{y}{L+x}$  at a distance  $y$ , from the centre-line of the nozzle, and  $x$  downstream of the reference plane.

The application of these two corrections to determine the conditions on an arbitrary position on a cone are carried out using the interpolation equations (C.8) from the cone table data using the following information for the basic parameters  $M$  and  $\theta_c$  and for the other freestream parameters. The freestream conditions (including  $M$ ) are taken as those that would exist at the same position in the test section if the model were removed. The cone angle to be used to apply the interpolation equations is taken to be  $\theta_c - \Delta\alpha$ . (For a model at zero incidence, referred to the nozzle centre-line, the correct application of the tables should be by using the values obtained on a cone of half-angle,  $\theta_c$ , at an angle of attack  $\Delta\alpha$ . However little improvement would be made for this interpretation, since  $\Delta\alpha$  is small compared to  $\theta_c$ ). The method has been shown to work well in the results and discussion of this report. The success is due to the closeness with which the bow-shock lies to the surface of the cone.

#### 4. Heat transfer rate predictions

##### Laminar

The Eckert reference (intermediate) enthalpy method is used (Ref. 4). The reference temperature,  $T^*$  is given by :

$$T^* = T_c + 0.5 (T_w - T_c) + 0.22 (T_r - T_c) \quad \text{C.15}$$



The equivalent perfect value of  $T_r$  is used in the calculation and hence the application of equation C.15 is equivalent to applying the reference enthalpy method.  $T_r$  is obtained from :

$$T_r = T_c + r \frac{u_c^2}{2c_p} \quad \text{C.16}$$

where  $r$  is the recovery factor having a value of  $P_r^{0.5}$  and  $P_r$  is the Prandtl number taken to have a value of 0.715.

The incompressible skin friction formula used was the Blasius equation :

$$c_f = 0.664/\sqrt{Re_s} \quad \text{C.17}$$

where  $c_f$  is the local skin friction and  $Re_s$  is the Reynolds number at station  $s$ .

The heat transfer rate can then be calculated from :

$$q = \rho^* u_c c_p \frac{c_f}{2} k_R (T_r - T_w) \quad \text{C.18}$$

where  $\rho^*$  is the density at the edge of the boundary layer calculated at the reference temperature  $T^*$ ,  $u_c$  is the velocity at the edge of the boundary layer,  $k_R$  is the Reynolds analogy parameter, and  $(T_r - T_w)$  is the driving temperature for the equation,  $c_f$  is the skin friction at reference temperature conditions.

For laminar flow,  $k_R$  is normally taken as  $Pr^{-2/3}$  and the skin friction coefficient, is calculated from equation 17. In this equation, the Reynolds number is given by :

$$Re_s = \frac{1}{k_M} \left\{ (Re_s)_{n-1} + \frac{\rho_c^* u_c}{\mu_c^*} \Delta s \right\} \quad \text{C.19}$$

$k_M$  is the Mangler transformation factor, used to transform a skin friction law from a two-dimensional to an axisymmetric case (the

flow over an axisymmetric body has a thinning action on the boundary layer).  $k_M$  has a value of 3 for laminar flow.

The term in the brackets is an accumulative Reynolds number, used in this varying flow field.  $(Re_s)_{n-1}$  is the accumulative Reynolds number at the last computation step,  $\Delta s$  is the step size.  $\rho_c^*$  and  $\mu_c^*$  are the density and viscosity of the flow on the cone calculated at the reference temperature.  $\mu_c^*$  is given by equation C.6.

### Turbulent

Two theories were used : the Sommer and Short reference enthalpy method (Ref. 17) and the Spalding-Chi method (Ref. 5).

The Sommer and Short method was applied in a very similar fashion to the laminar Eckert reference method. However the Sommer and Short reference temperature is given by :

$$T^* = T_c (1 + 0.035 M^2 + 0.45 (T_w/T_c - 1)) \quad C.20$$

The turbulent recovery temperature is given by :

$$T_r = T_c + (Pr)^{1/3} u_c^2 / 2c_p \quad C.21$$

The incompressible skin friction law used was the Karmann-Schoenherr implicit equation (Ref. ) :

$$\sqrt{c_f'} = \frac{0.242}{\log(Re_s c_f')} \quad C.22$$

$$\text{and } c_f = \frac{0.557 c_f'}{0.557 + 2(c_f')^{1/2}} \quad C.23$$

$c_f'$  is the average skin friction coefficient and  $c_f$  is the local skin friction coefficient. The above simple equation is a best

fit to the universal skin friction curve.

There is much uncertainty about the value of the Reynolds analogy factor,  $k_R$  (see Ref. ). An average value of  $k_R = 1.08$  was chosen for this study. In the turbulent version of equation C.19, the Mangler transformation factor,  $k_M$ , has a value of 2 (Ref. 4).

The Spalding-Chi method (Ref. 5) was applied by obtaining the local skin friction,  $c_f$ , from the tabulated data given in Ref. 5 using input values of  $Re_s$  (turbulent version of equation C.19),  $M_c$  and  $T' = T_w/T_c$ . A quadratic series was used to calculate  $C_f(Re_s)$ .

The heat transfer equation used was :

$$q_w = \rho_c u_c c_p \frac{c_f}{2} k_R (T_r - T_w)$$

-C8-

HEAT TRANSFER RATE ON CONE, RUN 265, AT 0.0 MSECS FROM PEAK,  
ALPHA= 0.0 DEGREES, TIP AT 0.001N ABOVE CENTRE LINE

# EQUIVALENT PERFECT CONDITIONS

T0 = 0.320483E 04 DEG K  
P0 = 0.683708E 05 PSI  
M = 0.200050E 02  
THETC = 0.500000E 02 DEG  
TW = 0.295000E 03 DEG K  
PR = 0.715000E 00

# FREE STREAM CONDITIONS (11) AT TIP OF CONE

T = 0.395462E 02 DEG K  
P = 0.142700E-01 PSI  
RHO = 0.162544E-04 SLUGS/FT\*\*3  
U = 0.841607E 04 FT/SEC  
MU = 0.508279E-07 LB\*SEC/FT\*\*2  
RE = 0.269140E 07

# CONE CONDITIONS AT TIP (EQUIVALENT PERFECT)

TE = 0.227814E 04 DEG K  
PE = 0.499599E 01 PSI  
RHOE = 0.988368E-04 SLUGS/FT\*\*3  
UE = 0.462182E 04 FT/SEC  
MOE = 0.132777E-05 LB\*SEC/FT\*\*2  
REE = 0.544037E 06  
ME = 0.144745E 01

NON-DIMENSIONAL PRESSURE COEFFTS. NEWTONIAN= 1.173, TANGENT CONE= 1.249  
SHOCK ANGLE TO SURFACE= 7.43 DEGREES  
REAL GAS VALUE, CP = 0.3884E 01

# CALCULATION OF HEAT TRANSFER IN ZERO PRESSURE GRADIENT

REYNOLDS ANALOGY FACTOR = 1.100  
REF. TEMP., ECKERT = 1464.1, SOM-SHORT = 1552.7 DEG K

X	Q BTU/SEC/FT**2		CFKS	
	TURBULENT		TURBULENT	
				Q BTU/SEC/FT**2
				LAMINAR
0.500	0.131718E 03	0.876370E-02	0.121495E 03	
1.000	0.111488E 03	0.741775E-02	0.859104E 02	
1.500	0.101586E 03	0.675890E-02	0.701455E 02	
2.000	0.952803E 02	0.633935E-02	0.607478E 02	
2.500	0.907552E 02	0.603828E-02	0.543345E 02	
3.000	0.872758E 02	0.580677E-02	0.496004E 02	
3.500	0.844764E 02	0.562052E-02	0.459210E 02	
4.000	0.821512E 02	0.546582E-02	0.429552E 02	

# CALCULATION WITH CORRECTION FOR CONICITY

X IN	RE	PE	CP(NEWT)	CP(TC)	Q(LAM)	Q(S-S)	Q(S-C)	THETS
0.500	0.1438E 05	4.25	1.152	1.226	120.081	130.145	73.086	7.34
1.000	0.2885E 05	4.72	1.131	1.203	83.890	108.779	64.908	7.25
1.500	0.4344E 05	4.59	1.110	1.181	67.665	97.861	60.609	7.16
2.000	0.5811E 05	4.46	1.089	1.159	57.882	90.610	57.724	7.07
2.500	0.7287E 05	4.34	1.069	1.137	51.131	85.187	55.558	6.98
3.000	0.8772E 05	4.22	1.050	1.116	46.093	80.847	53.820	6.89
3.500	0.1026E 06	4.10	1.030	1.095	42.136	77.218	52.365	6.81
4.000	0.1177E 06	3.99	1.011	1.074	38.913	74.088	51.109	6.72

# APPENDIX D

## Heat Transfer on a Sphere and a Blunt 50° Half-Angle Cone

### Stagnation point heat transfer

The theory of Fay and Riddell (Ref. 1) is used to predict the stagnation point heat transfer. The formula used is :

$$q = 0.763 \text{ Pr}^{-0.6} (\rho_e \mu_e)^{0.5} \left( \frac{\rho_e \mu_e}{\rho_w \mu_w} \right)^{0.1} \left( \frac{du}{ds} \right)_0^{1/2} [h_e - h_w]$$

Using a modified Newtonian theory, the velocity gradient at the stagnation point of a body with radius,  $R_N$ , is given by :

$$\left( \frac{du}{ds} \right)_0 = \frac{1}{R_N} \sqrt{\frac{2p_{t2}}{\rho_e}}$$

where  $p_{t2}$  is the stagnation pressure. Subscript e refers to conditions just outside the boundary layer, subscript w to wall conditions and subscript 0 to the stagnation point.

The total enthalpy  $h_e$  was assumed equal to the value in the nozzle reservoir, calculated for real nitrogen from the measurements of  $p_0$  and  $T_0$ . The wall enthalpy  $h_w$  was taken with sufficient accuracy to correspond to  $T_w = 293^\circ\text{K}$ . The viscosity of nitrogen was found from Sutherland's formula (Eqn. C.6) with the value of  $T_e$ , the static temperature behind the shock calculated from  $h_e$  taking into account the departure from a perfect gas due to vibrational excitation (Ref. 14). The stagnation point pressure,  $p_{t2}$ , was measured and the densities  $\rho_e$ ,  $\mu_w$  were then obtained from  $p_{t2}$  and  $T_e$ ,  $T_w$  using the perfect gas law. A Prandtl number of 0.715 was assumed.

Curves taken from the Lees similarity theory (Ref. 3) are used to predict the heat transfer rate, in relation to the stagnation point heat transfer downstream of the stagnation point for these body shapes.

TABLE 1. POSITION OF INSTRUMENTATION

MODELS A, B, D & E ARE GIVEN IN FIG 2.

MODEL C

GAUGE	1	2	3	4	5	6	7	8	10	12
S in	0.36	.895	1.395	1.895	2.395	2.895	3.395	4.395	5.395	6.395
S/R <sub>n</sub>	0.48	1.191	1.760	2.53	3.19	3.86	4.52	5.85	7.19	8.52

TABLE 2 SUMMARY OF TEST CONDITIONS AT NOSE OF MODELS  
AT TIME  $T = 0$  msec FROM PEAK

RUN	MODEL	INCIDENCE	RESERVOIR		PITOT	M	$Re \times 10^{-6}$	QD	Q
			$P_0$	$T_0$					
204	A	0	58,900	2400	8.2	19.7	3.03	630	69.0
205	A	0	59,400	2485	7.45	20.0	2.69	575	68.7
206	A	-10°	57,800	2375	-	-	-	-	-
207	A	-10°	57,900	2380	7.40	20.1	2.91	571	64.9
208	A	+10°	56,900	2330	7.55	20.0	3.04	581	63.8
209	A	0	32,500	2137	4.50	19.27	2.12	346	41.7
210	A	0	39,600	2288	5.48	19.30	2.24	422	50.9
211	B	0	57,900	2422	7.08	20.17	2.74	546	54.8
212	B	0	30,960	2138	4.24	19.25	2.01	326	40.3
213	B	0	40,100	2270	5.55	19.34	2.31	428	50.9
214	B	0	57,200	2540	26.3	15.21	4.96	2032	131.7
284	C	0	57,600	2420	7.8	19.8	2.87	600	67.7
285	C	-10°	58,300	2405	8.1	19.7	2.98	622	68.7
286	C	+10°	59,300	2420	7.8	19.9	2.91	600	68.0
287	C	0	37,600	2246*	5.0	19.5	2.16	383	47.2
288	D	0	59,300	2450	8.5	19.5	2.98	658	72.2
289	D	0	37,600	2246*	4.7	19.7	2.11	364	46.1
290	E	0	58,340	2400	8.4	19.6	3.04	646	70.0
291	E	0	37,600	2226	5.4	19.2	2.29	413	48.6
292	E	0	57,100	2350	29.2	15.1	6.14	2253	127.0

\* Estimate - measurement not taken  
Units  $P_0$  and pitot in  $lb/in^2$ ; dynamic pressure  $q_d$  in  $lb/ft^2$   
 $T_0$  in  $^{\circ}K$ ;  $Re$  in  $ft^{-1}$ ; stagnation point heat transfer,  $Q$ ,  
in  $Btu / ft^2 sec$ .

LONGSHOT TEST CONDITIONS, RUN NO.285 AT 7.6 IN. FROM NOZZLE EXIT,  
AND 4.6 FROM CENTRELINE

T(MS) MACH NO P(PSI) QD(LB/FT**2)	PO(PSI) POP(PSI) T(K) Q(BTU)	TO(K) TOP(K) RHO TT2R(K)	PITOT(PSI) RE/FT V(FT/SEC) CONDENSATION
0.000	0.583408E 05	0.240516E 04	0.896696E 01
19.718	0.688585E 05	0.309855E 04	0.297866E 07
0.158789E-01	0.393400E 02	0.181817E-04	0.827392E 04
0.622343E 03	0.687024E 02	0.264564E 04	0.359004E 02

LONGSHOT TEST CONDITIONS, RUN NO.291 AT 7.2 IN. FROM NOZZLE EXIT,  
AND 4.4 FROM CENTRELINE

T(MS) MACH NO P(PSI) QD(LB/FT**2)	PO(PSI) POP(PSI) T(K) Q(BTU)	TO(K) TOP(K) RHO TT2R(K)	PITOT(PSI) RE/FT V(FT/SEC) CONDENSATION
0.000	0.376553E 05	0.222620E 04	0.536936E 01
19.208	0.402278E 05	0.274521E 04	0.229039E 07
0.111158E-01	0.367024E 02	0.136425E-04	0.778524E 04
0.413437E 03	0.485692E 02	0.231505E 04	0.346679E 02

LONGSHOT TEST CONDITIONS, RUN NO.292 AT 8.5 IN. FROM NOZZLE EXIT,  
AND 4.9 FROM CENTRELINE

T(MS) MACH NO P(PSI) QD(LB/FT**2)	PO(PSI) POP(PSI) T(K) Q(BTU)	TO(K) TOP(K) RHO TT2R(K)	PITOT(PSI) RE/FT V(FT/SEC) CONDENSATION
0.000	0.570779E 05	0.234936E 04	0.292399E 02
15.125	0.682901E 05	0.392094E 04	0.613917E 07
0.976932E-01	0.646000E 02	0.681124E-04	0.813361E 04
0.225301E 04	0.126923E 03	0.256365E 04	0.437353E 02

TABLE 3 TYPICAL TEST SECTION CONDITIONS



TABLE 4 HEAT TRANSFER MEASUREMENTS ON MODEL A,

TIME  $T = 0$  m.secs,  $M = 20$  (B.Th.u./ft<sup>2</sup>sec.)

RUN NO	204	205	206	207	208	209	210
INCIDENCE	0°	0°	-10°	-10°	+10°	0°	0°
TEST CASE	HIGH RE	HIGH RE	HIGH RE	HIGH RE	HIGH RE	LOW RE <sub>1</sub>	LOW RE <sub>2</sub>
GAUGE 1	122.4	121.5	105.7	100.0	124.2	69.4	91.0
GAUGE 2	72.9	74.1	66.3	57.7	80.5	42.6	51.0
GAUGE 3	61.2	64.2	54.8	54.2	69.3	34.2	46.3
GAUGE 4	58.7	61.2	56.0	52.0	60.0	36.0	42.2
GAUGE 5	54.0	59.3	-	46.7	62.3	31.7	36.3
GAUGE 6	49.4	52.2	-	39.0	-	-	27.0
GAUGE 7	40.9	37.0	39.3	28.6	51.5	24.6	40.2
GAUGE 8	6.0	6.1	1.7	12.1	9.5	3.7	2.92
GAUGE 10	2.4	0.8	0.6	4.4	3.5	0.9	1.27
GAUGE 12	4.0	2.8	1.9	4.8	7.2	2.1	4.2

-D5-

TABLE 5 HEAT TRANSFER MEASUREMENTS ON MODEL B. ZERO INCIDENCE  
TIME  $T = 0$  H.secs  $M = 20, 15$  (B.Th.u./ft<sup>2</sup>sec.)

TEST CASE	211		212		213		214	
	HIGH RE		LOW RE <sub>1</sub>		LOW RE <sub>2</sub>		M = 15	
GAUGE 1	-		-		-		-	
GAUGE 2	42.3		20.9		40.2		107.3	
GAUGE 3	65.0		39.4		45.6		164.5	
GAUGE 4	64.2		31.6		42.9		158.4	
GAUGE 5	61.2		37.7		51.7		176.2	
GAUGE 6	41.8		23.4		27.8		112.6	
GAUGE 7	70.0		37.1		49.0		185.0	
GAUGE 8	11.1		5.8		7.4		26.9	
GAUGE 10	4.1		2.3		2.8		13.5	
GAUGE 12	3.5		1.7		1.8		11.4	

TABLE 6 HEAT TRANSFER MEASUREMENTS ON MODEL C

TIME T = 0 msec M = 20 (Btu/ft<sup>2</sup>sec)

RUN NO	284	285	286	287
INCIDENCE	0	-10	+10	0
TEST CASE	HIGH RE	HIGH RE	HIGH RE	LOW RE
GAUGE 0	142.7	141.7	149.7	86.1
GAUGE 1	100.7	71.8	107.0	63.0
GAUGE 2	81.8	56.4	93.3	47.6
GAUGE 3	63.3	41.2	67.6	33.3
GAUGE 4	57.3	43.5	66.3	34.6
GAUGE 5	47.1	34.8	57.5	28.3
GAUGE 6	48.1	32.8	50.4	26.9
GAUGE 7	46.1	32.2	49.5	25.9
GAUGE 8	6.4	3.5	10.6	4.5
GAUGE 12	3.4	0.8	8.1	0.8

TABLE 7 HEAT TRANSFER MEASUREMENTS ON MODELS D & E

TIME T = 0 m secs. M = 20(15) (B.Thu/ft<sup>2</sup>sec)

RUN NO	288	289	290	291	292
TEST CASE	HIGH RE	LOW RE	HIGH RE	LOW RE	M = 15
MODEL	D	D	E	E	E
GAUGE - 1	90.6	60.9	95.0	82.0	202.6
GAUGE 2	90.2	63.6	75.2	61.0	179.6
GAUGE 3	62.7 *	52.2	81.7	63.2	217.7
GAUGE 4	66.3	47.3	58.4	46.3	152.3
GAUGE 5	43.3	32.7	53.8	40.9	151.7
GAUGE 6	35.9	25.5	26.5	20.3	80.5
GAUGE 7	22.8	15.6	22.9	17.5	70.7
GAUGE 8	18.4	11.5	18.7	22.5	65.5
GAUGE 9	9.9	8.2	13.9	6.4	35.2
GAUGE 10	7.8	4.6	9.7	4.0	13.4

\* suspect reading - scope in uncalibrated position

TABLE 8 PRESSURE MEASUREMENTS ON MODEL A. TIME T = 0 asecs.  
M = 20, (lb/in<sup>2</sup>)

RUN NO	204	205	206	207	208	209	210
INCIDENCE	0°	0°	+10°	+10°	-10°	0°	0°
TEST CASE	HIGH RE	HIGH RE	HIGH RE	HIGH RE	HIGH RE	LOW RE <sub>1</sub>	LOW RE <sub>2</sub>
PITOT	8.2	7.45	-	7.40	7.55	4.50	5.48
GAUGE 1	5.4	5.1	-	6.6	3.3	2.8	3.2
GAUGE 2	5.3	5.0	-	6.5	3.5	2.9	3.5
GAUGE 3	5.2	4.9	-	6.3	3.3	2.8	3.2
GAUGE 5	5.1	4.7	-	6.3	3.3	2.8	3.3
GAUGE 6	4.95	4.6	-	5.9	3.2	2.7	3.4
GAUGE 7	4.7	4.5	-	5.8	3.0	2.8	2.8
GAUGE 8	0.32	0.31	-	0.68	0.08	0.18	0.20

TABLE 9 PRESSURE MEASUREMENTS ON MODEL B, TIME T = 0 msec  
M = 20, 15. ZERO INCIDENCE (lb/in<sup>2</sup>)

RUN NO TEST CASE	211		212		213		214	
	HIGH RE		LOW RE <sub>1</sub>		LOW RE <sub>2</sub>		M = 15	
PITOT	7.1		4.2		5.5		26.3	
GAUGE 1	5.1		4.0		2.0		17.7	
GAUGE 2	5.7		3.2		1.9		18.4	
GAUGE 3	4.5		2.2		1.4		15.3	
GAUGE 4	4.4		3.1		3.0		16.2	
GAUGE 5	5.1		2.9		3.1		14.1	
GAUGE 6	4.9		2.7		3.1		15.6	
GAUGE 7	4.1		2.4		2.8		15.6	
GAUGE 8	0.31		0.18		0.23		1.1	

TABLE 10 PRESSURE MEASUREMENTS ON MODEL C, TIME T = 0 msec  
M = 20 (lb/in<sup>2</sup>)

RUN NO INCIDENCE TEST CASE	284		285		286		287	
	0	HIGH RE	+10°	HIGH RE	-10°	HIGH RE	0	LOW RE
PITOT	6.75		7.9		7.54		4.73	
GAUGE 1	4.9		6.9		4.1		3.77	
GAUGE 2	4.3		6.3		2.8		2.78	
GAUGE 3	4.1		6.1		3.2		2.83	
GAUGE 4	4.3		6.4		3.4		2.93	
GAUGE 5	4.3		6.1		3.2		2.80	
GAUGE 6	4.2		5.7		3.2		2.81	
GAUGE 7	4.3		5.8		3.2		2.91	

TABLE 11 PRESSURE MEASUREMENTS ON MODEL D & E, TIME T = 0 msec  
M = 20(15) (lb/in<sup>2</sup>)

RUN NO	288	289	290	291	292
TEST CASE	HIGH RE	LOW RE	HIGH RE	LOW RE	M = 15
MODEL	D	D	E	E	E
PITOT	8.35	4.55	8.24	5.3	29.2
GAUGE 1	7.4	4.3	8.1	5.0	27.1
GAUGE 2	6.7	3.6	6.9	4.1	24.9
GAUGE 3	5.5	3.2	5.6	3.56	20.4
GAUGE 4	4.2	2.6	4.5	2.89	16.9
GAUGE 5	3.2	1.98	3.1	2.03	11.7
GAUGE 7	1.45	0.93	1.39	0.82	4.5
GAUGE 9	0.46	0.31	0.47	0.30	1.46

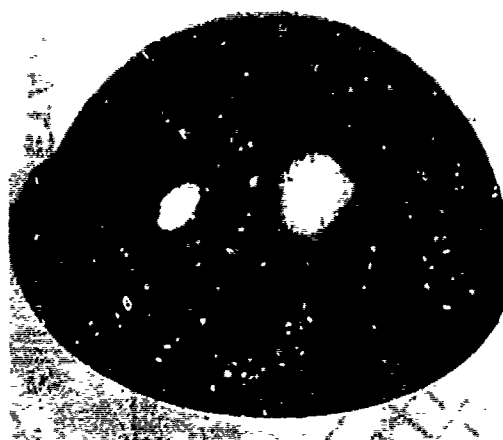




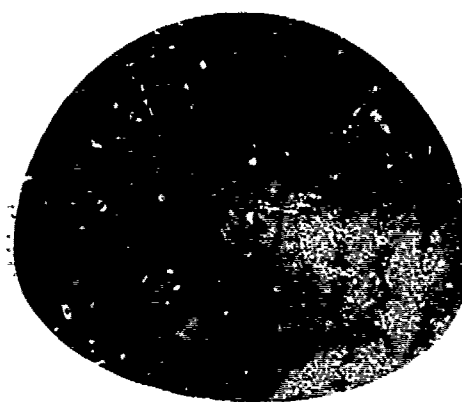
MODEL B



MODEL C

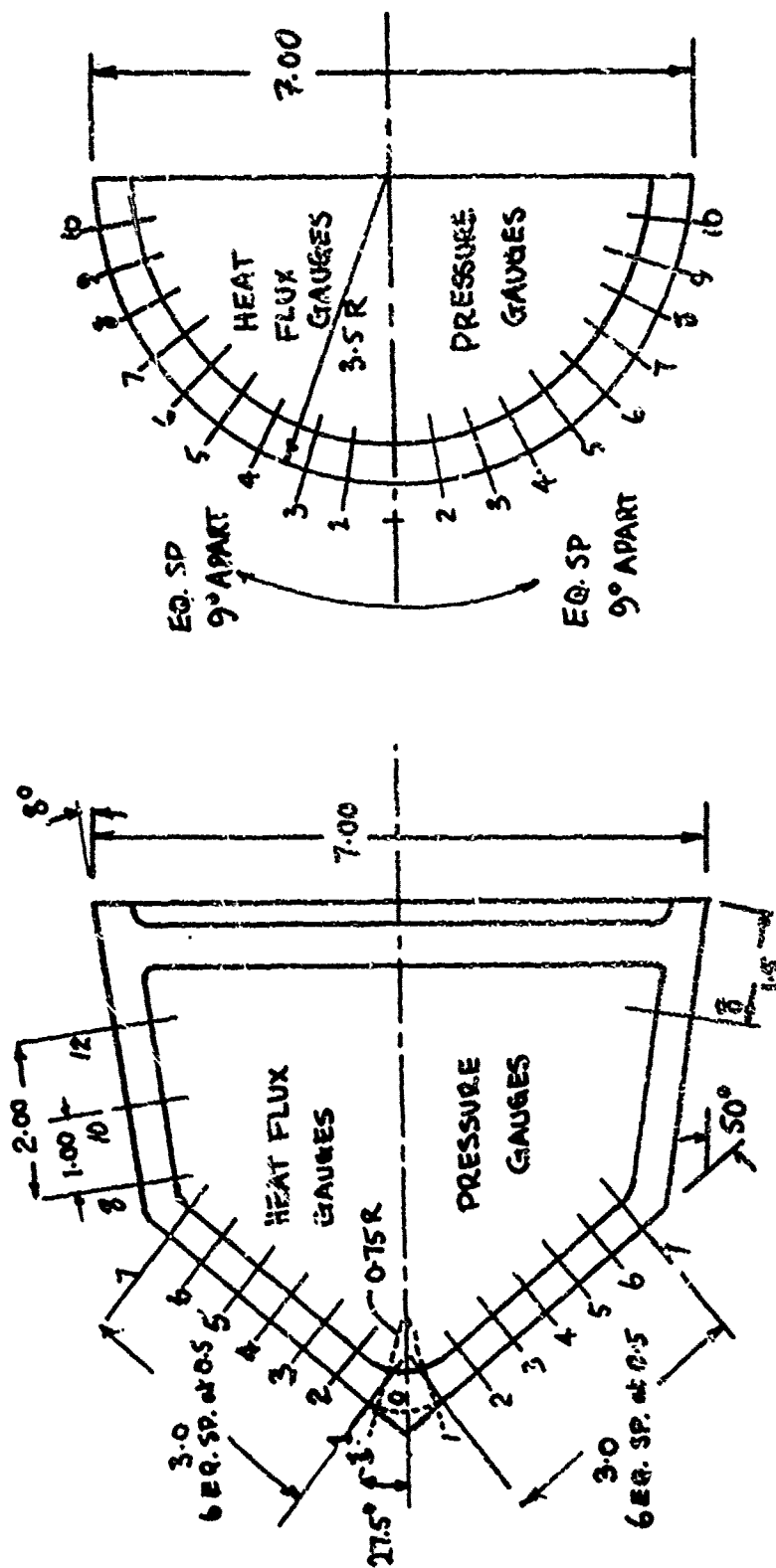


MODEL D



MODEL E

FIG 1. FOUR OF THE MODELS TESTED



MODELS D & E

MODELS A, B & C

FIG. 2 DETAILS OF MODELS

-D15-

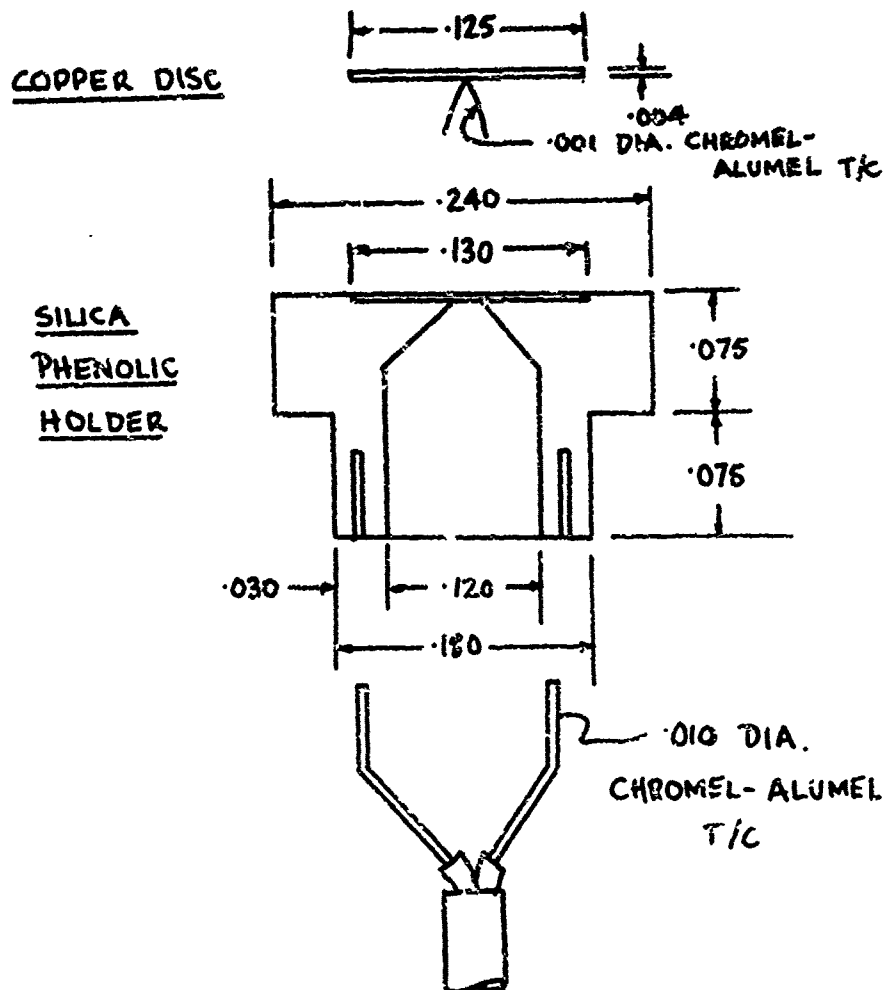


FIG. 3 HEAT FLUX GAUGE ASSEMBLY

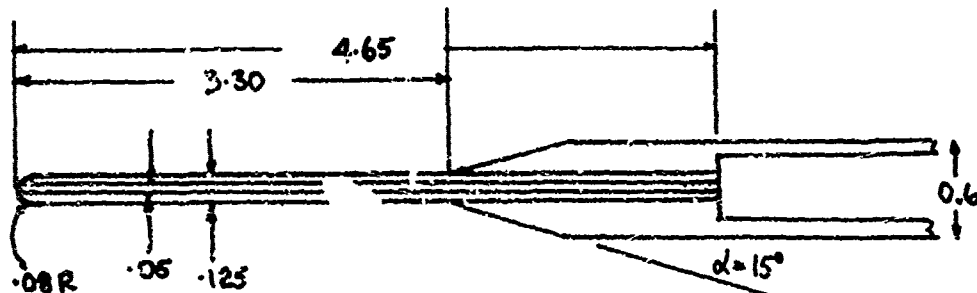
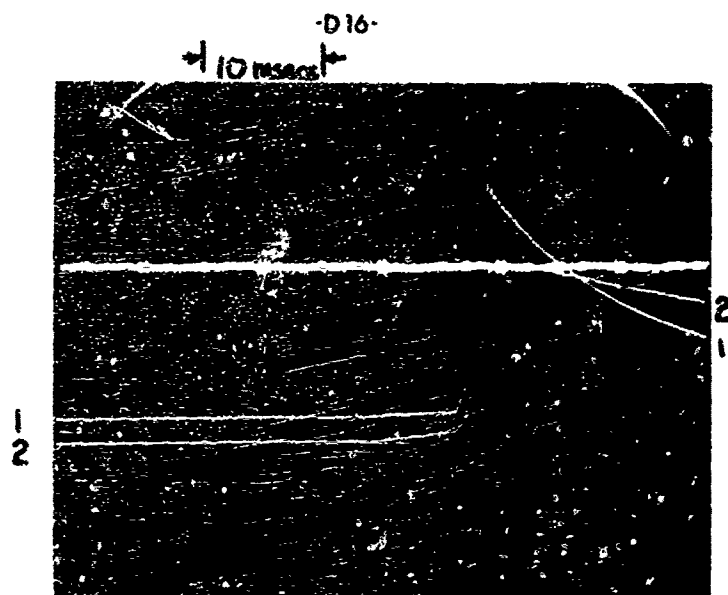
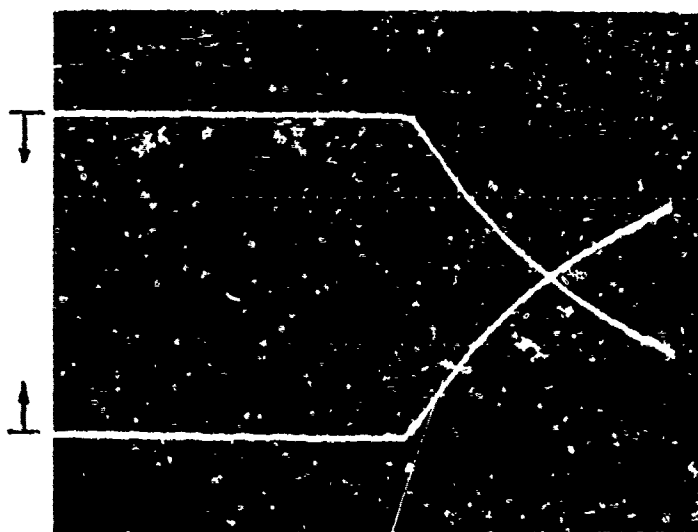


FIG 4 PITOT PROBE GEOMETRY



1. RESERVOIR PRESSURE    2. RESERVOIR TEMPERATURE



CALORIMETRIC HEAT TRANSFER TRACES

FIG 5 TYPICAL TRACES FROM INSTRUMENTATION



FIG. 6 THE LONGSHOT WIND TUNNEL



FIG. 7 MODEL E MOUNTED IN TEST SECTION



204



205



206



207



209



210

a) MODEL A  
FIG 8 SCHLIEREN PHOTOGRAPHS



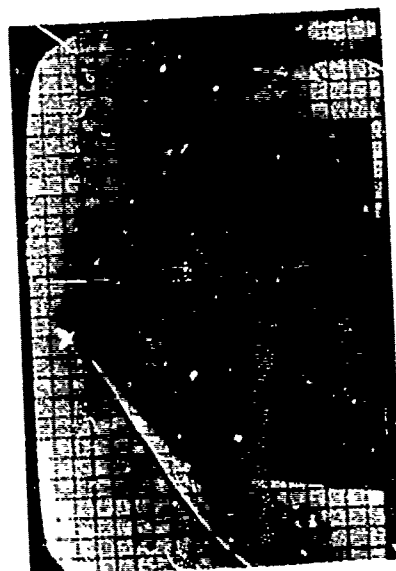
211



212



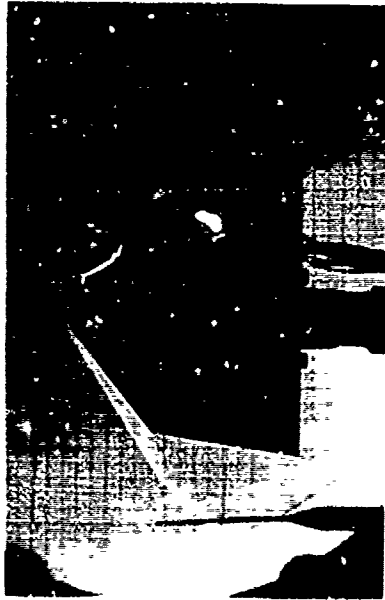
213



214

b) MODEL B

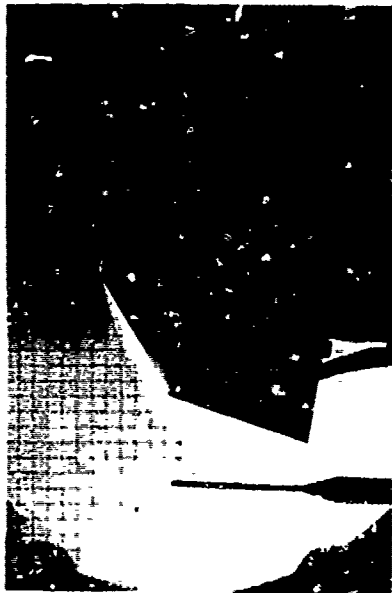
FIG. 8 SCHLIEREN PHOTOGRAPHS



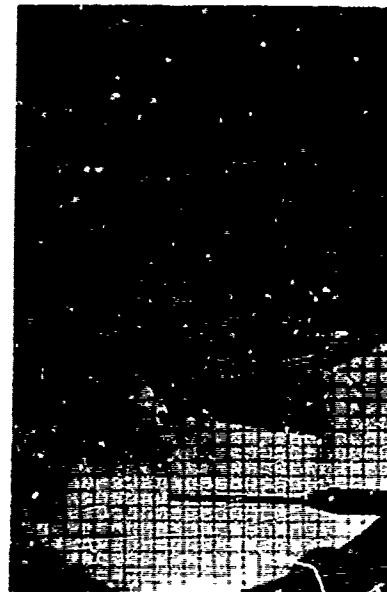
284



285



286



287

c) MODEL C

FIG. 8 SCHLIEREN PHOTOGRAPHS





288

d) MODEL D



289



290

291

292

e) MODEL E

FIG 3 SCHLIEREN PHOTOGRAPHS

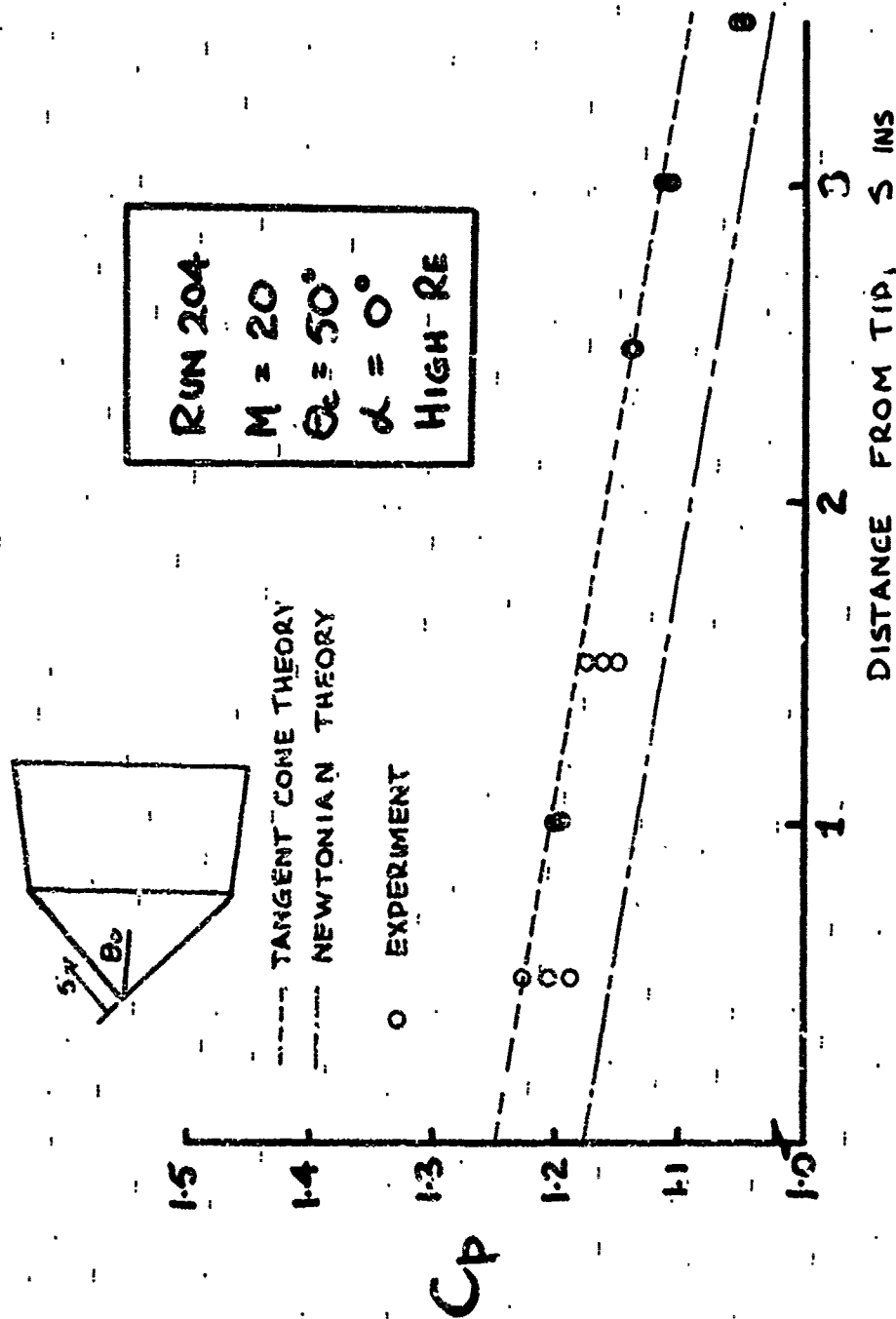


FIG 9 PRESSURE DISTRIBUTION ON MODEL A

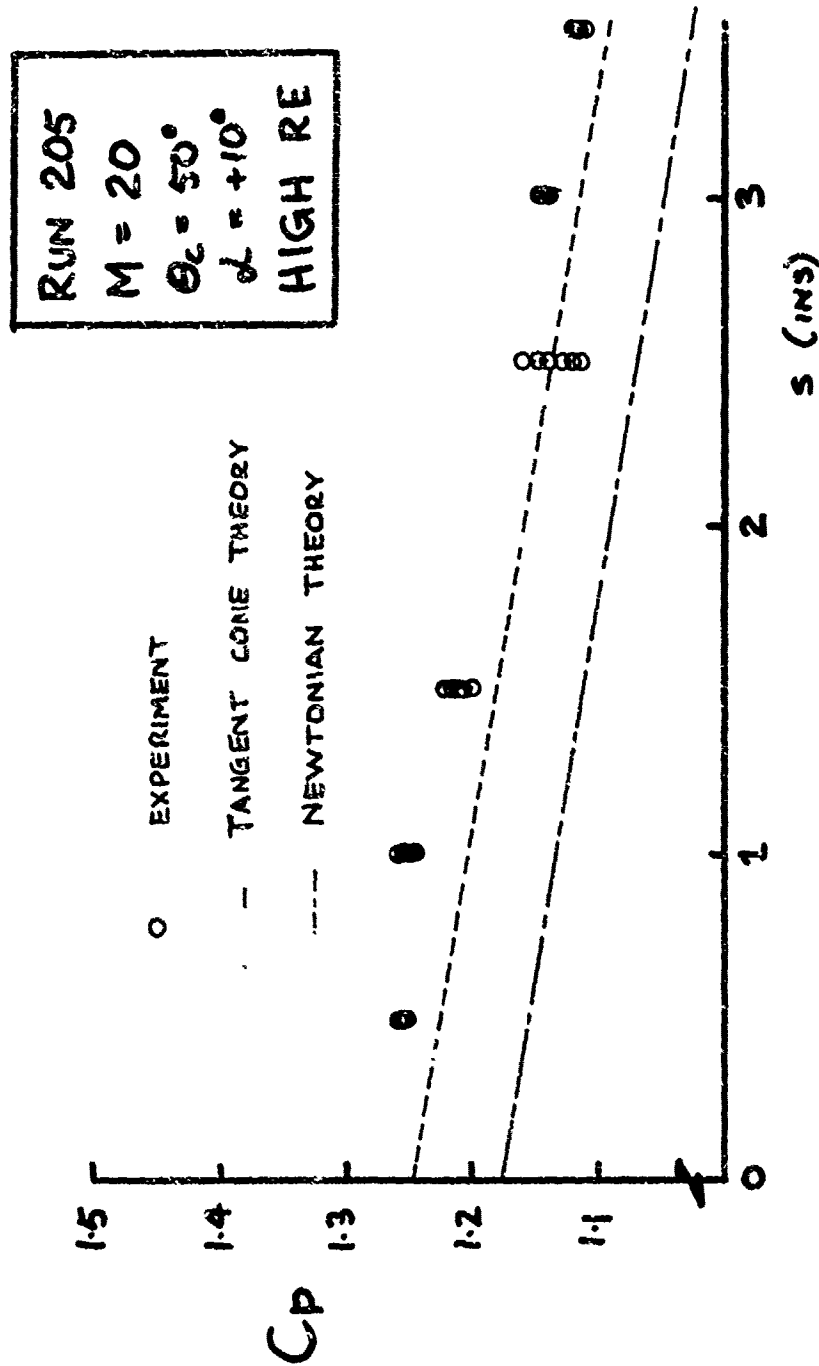


FIG. 10 PRESSURE DISTRIBUTION ON MODEL A

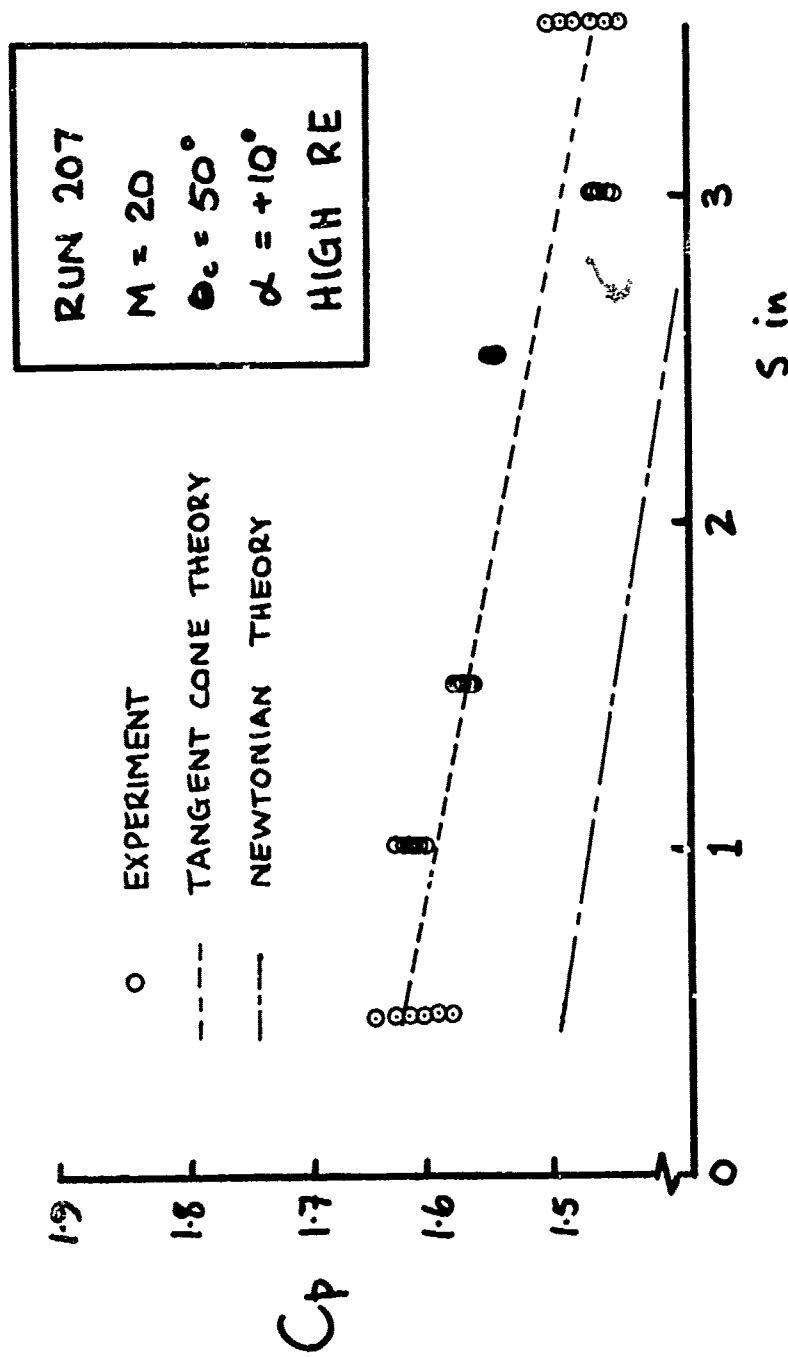


FIG 11 PRESSURE DISTRIBUTION ON MODEL A

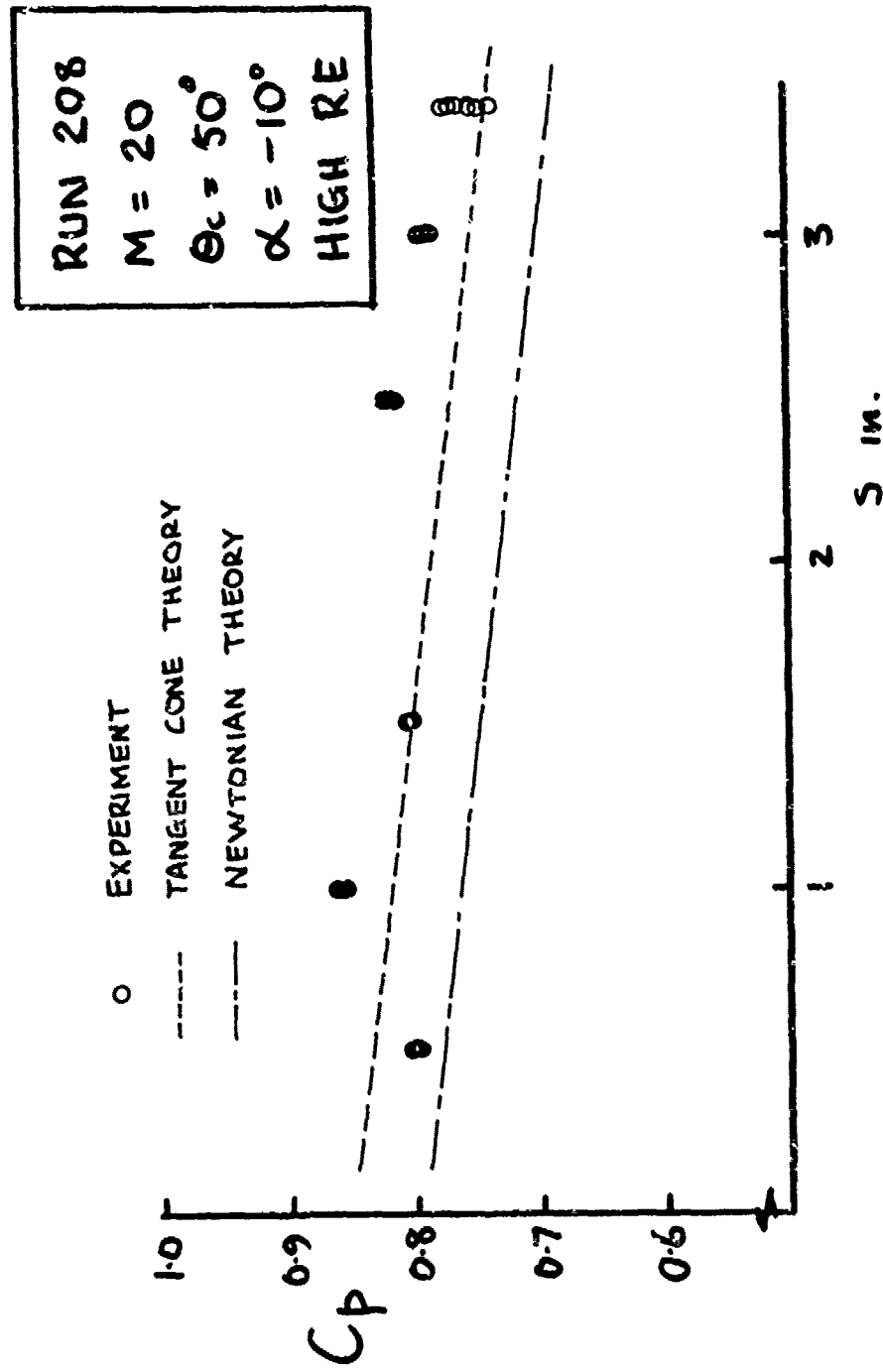


FIG. 12 PRESSURE DISTRIBUTION ON MODEL A

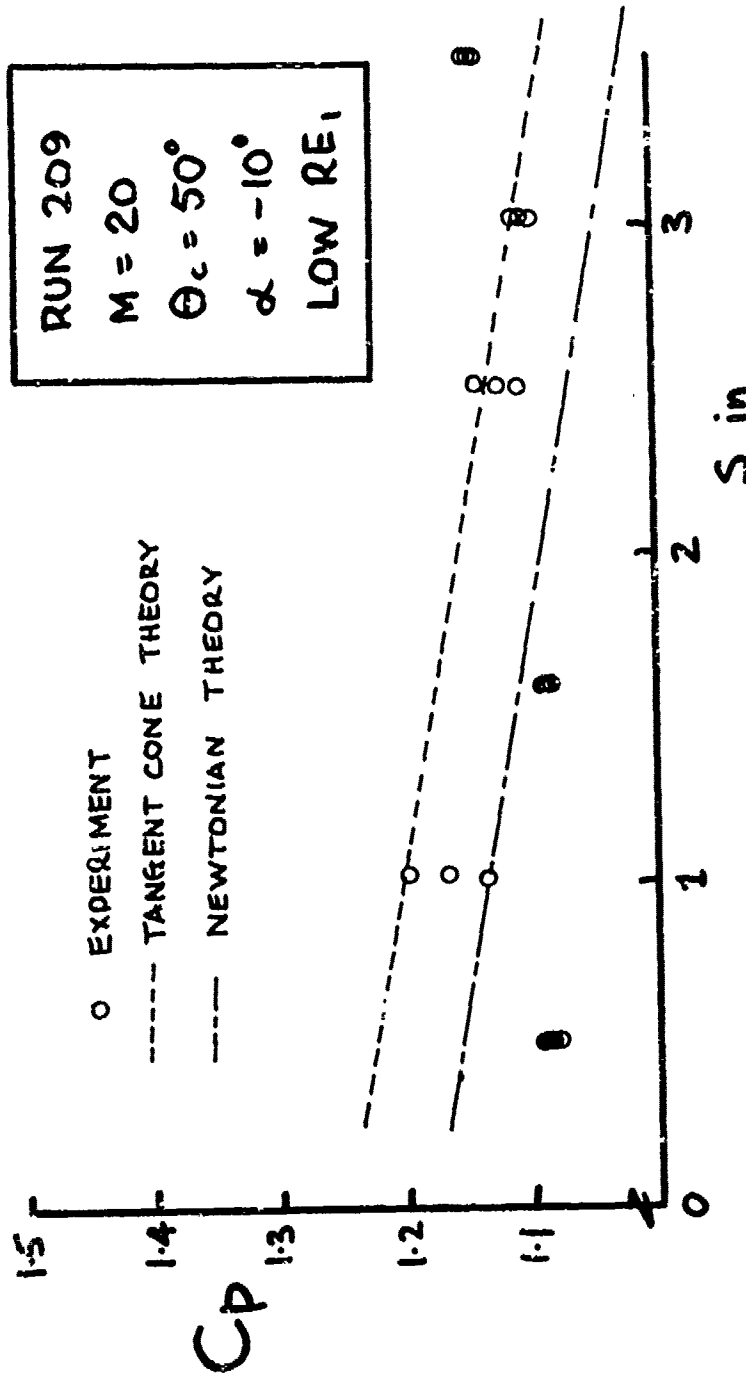


FIG 13 PRESSURE DISTRIBUTION ON MODEL A

**THIS  
PAGE  
IS  
MISSING  
IN  
ORIGINAL  
DOCUMENT**

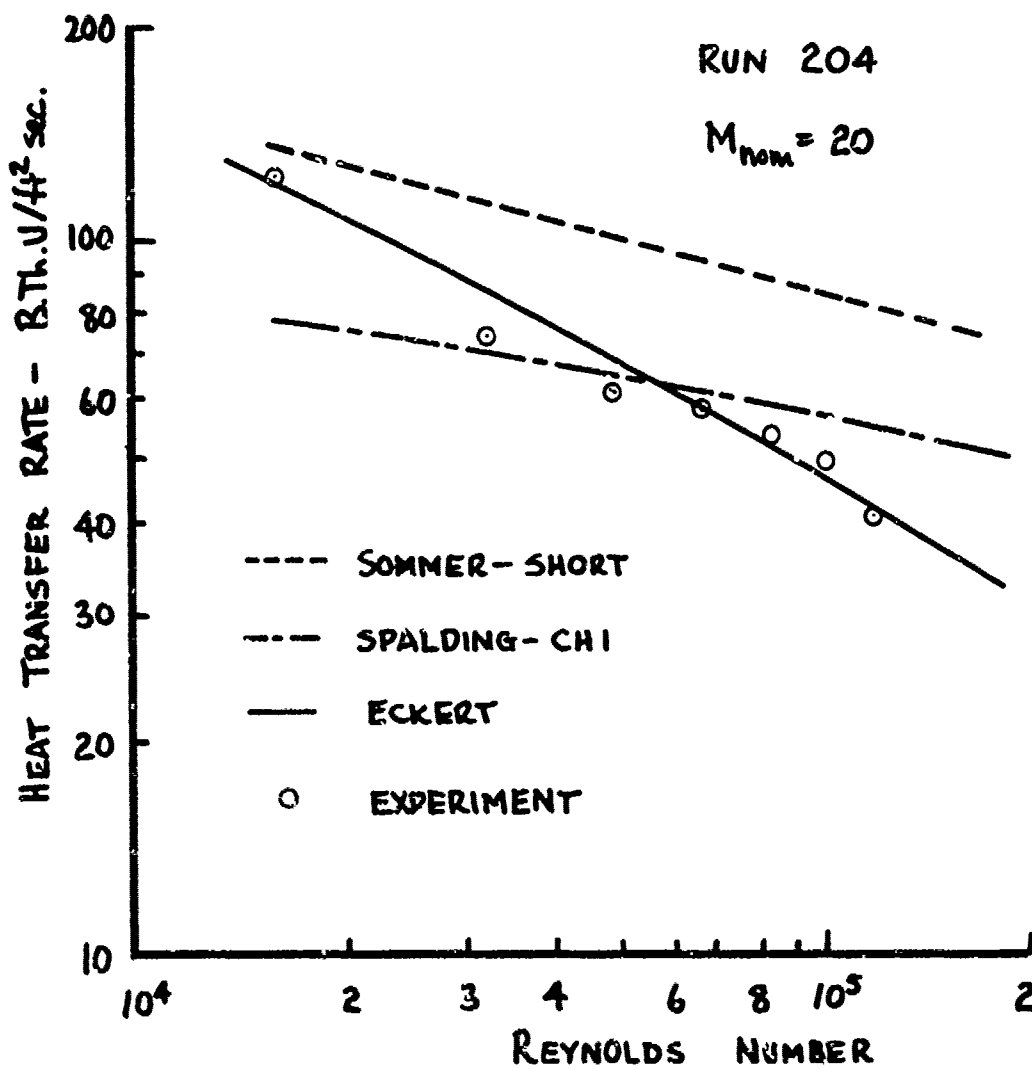


FIG. 15 HEAT TRANSFER ON MODEL A AT ZERO INCIDENCE

a) FIRST HIGH RE CASE



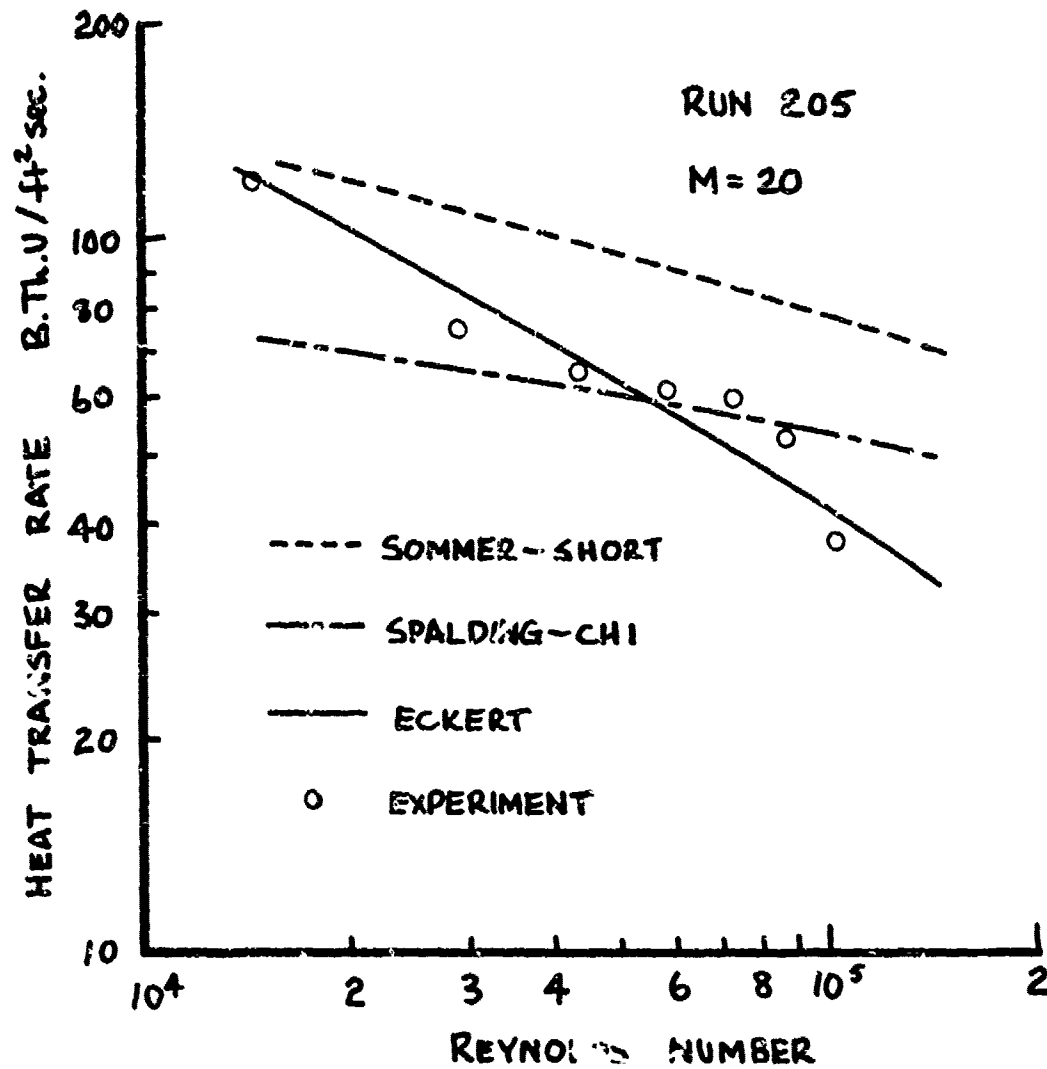


FIG. 15(b) HEAT TRANSFER RATE ON MODEL A AT ZERO INCIDENCE

b) 2<sup>nd</sup> HIGH REYNOLDS NO. CASE

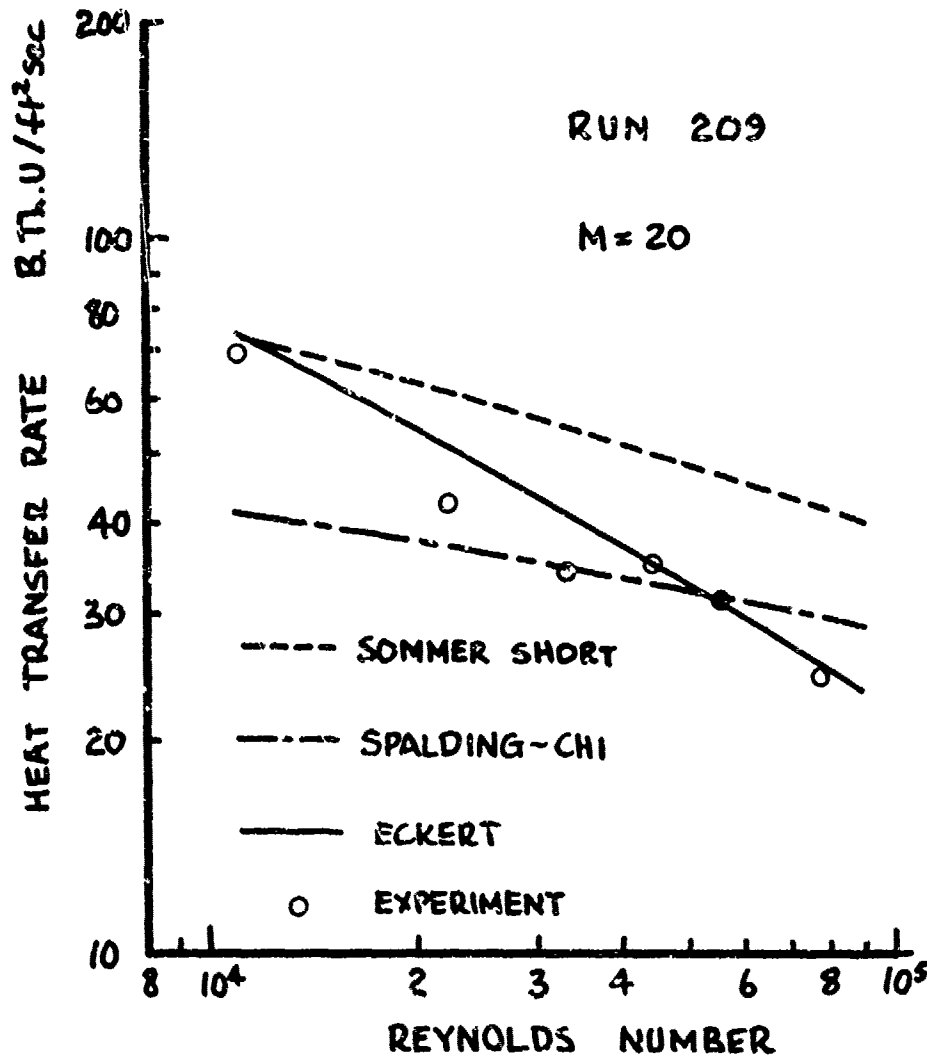


FIG. 15 (cont.) HEAT TRANSFER RATE ON MODEL A  
AT ZERO INCIDENCE

c) 1<sup>ST</sup> LOW RE CASE

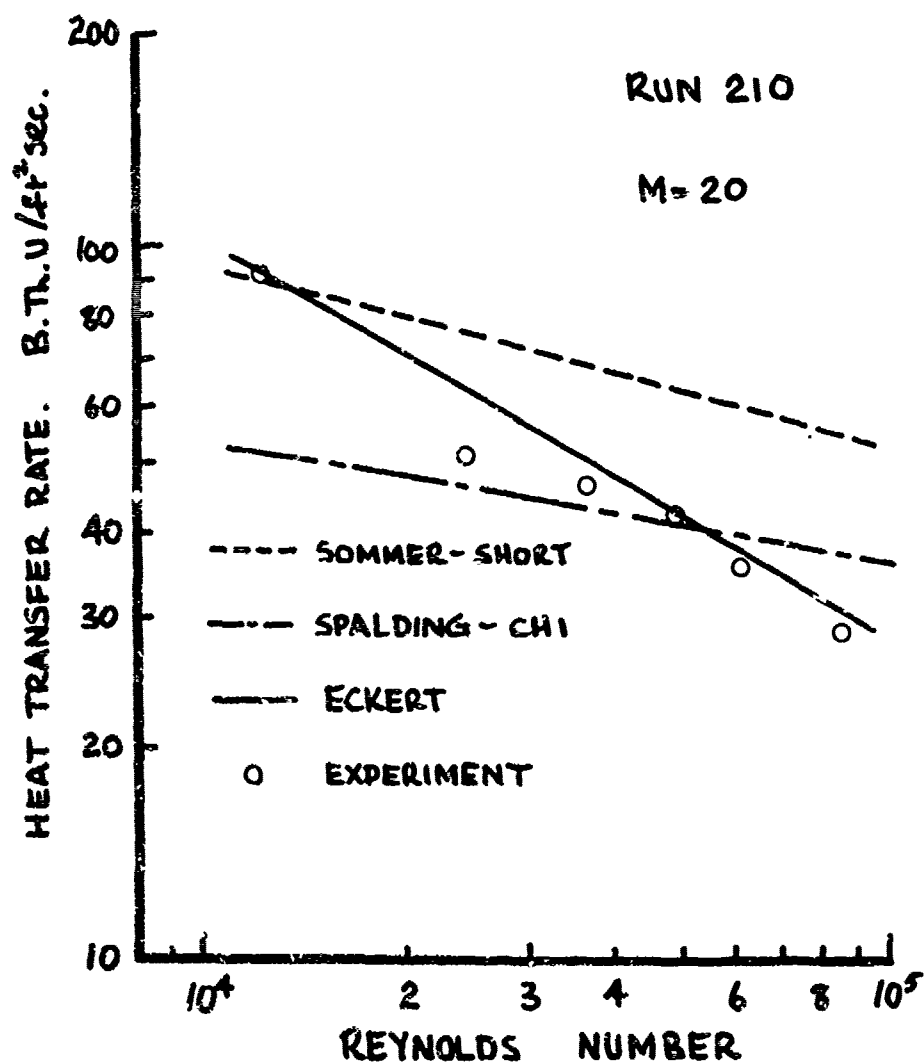


FIG. 15(cont.) HEAT TRANSFER RATE ON MODEL  
A AT ZERO INCIDENCE

a) 2<sup>nd</sup> LOW REYNOLDS NUMBER CASE

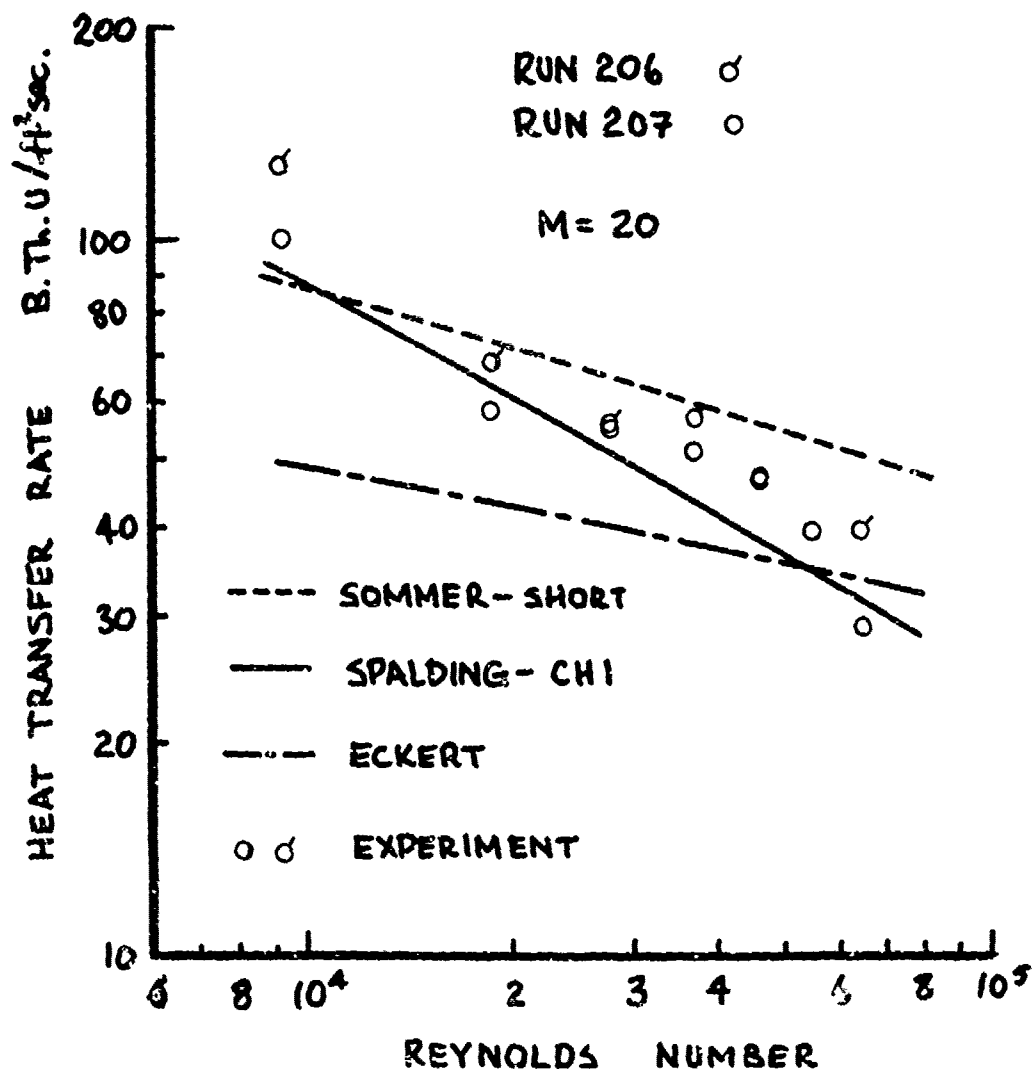


FIG. 16 HEAT TRANSFER RATE ON MODEL A AT  $\alpha = +10^\circ$

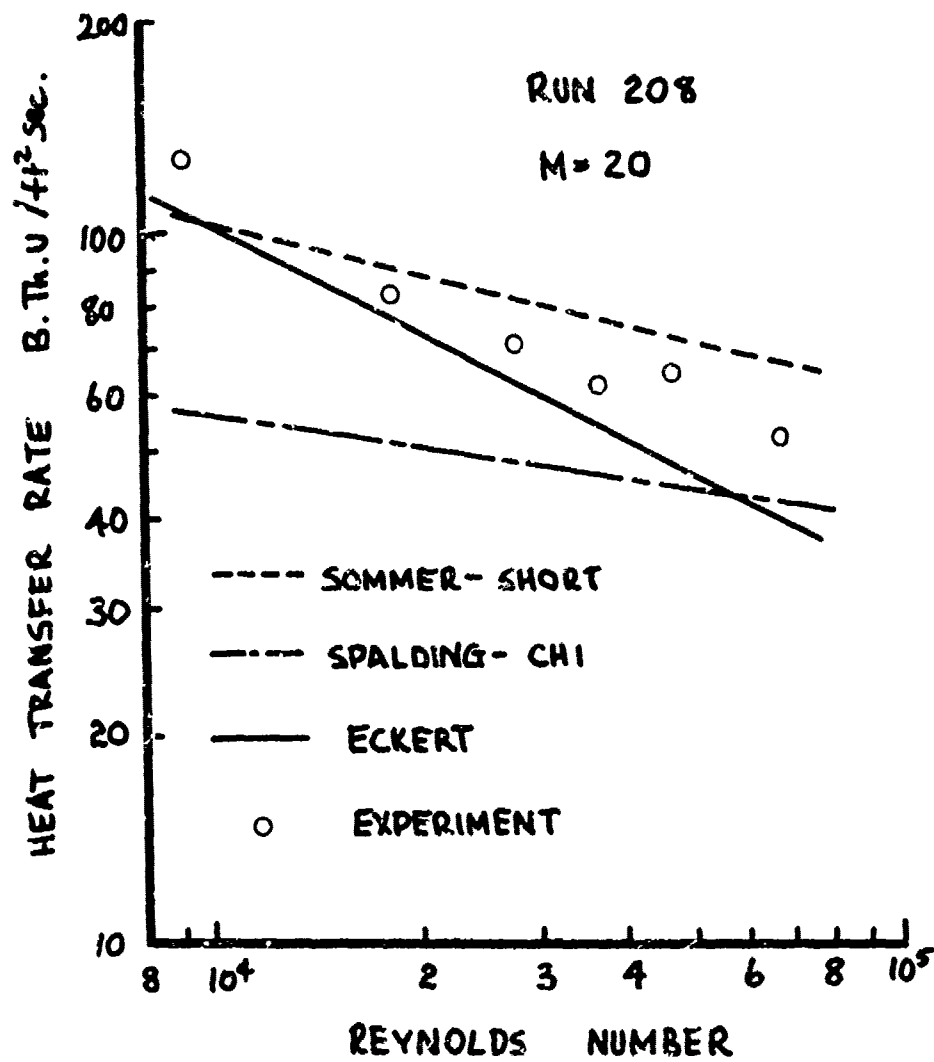


FIG. 17 HEAT TRANSFER RATE ON MODEL A AT  $\alpha = -10^\circ$

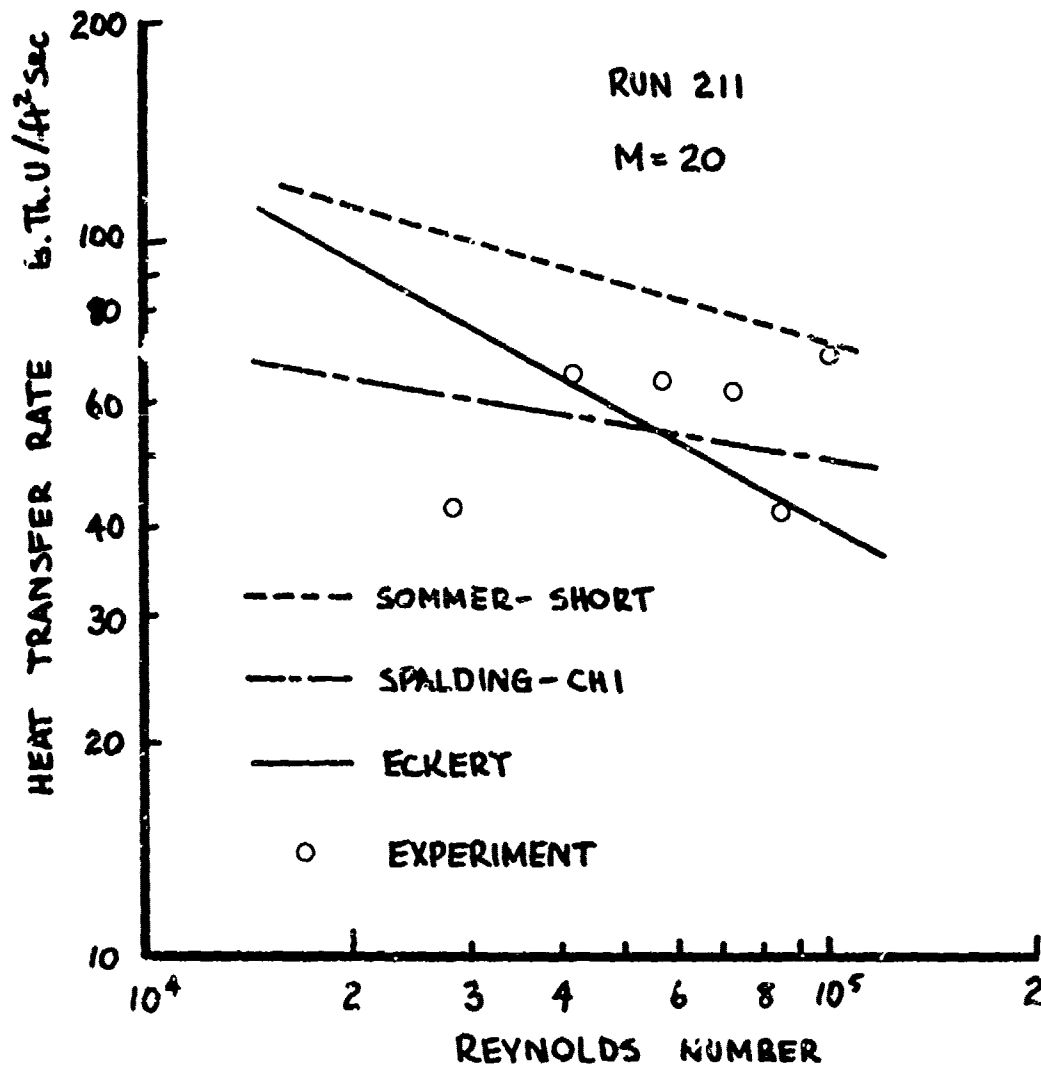


FIG. 18 HEAT TRANSFER ON ROUGH MODEL B AT  
HIGH RE CASE

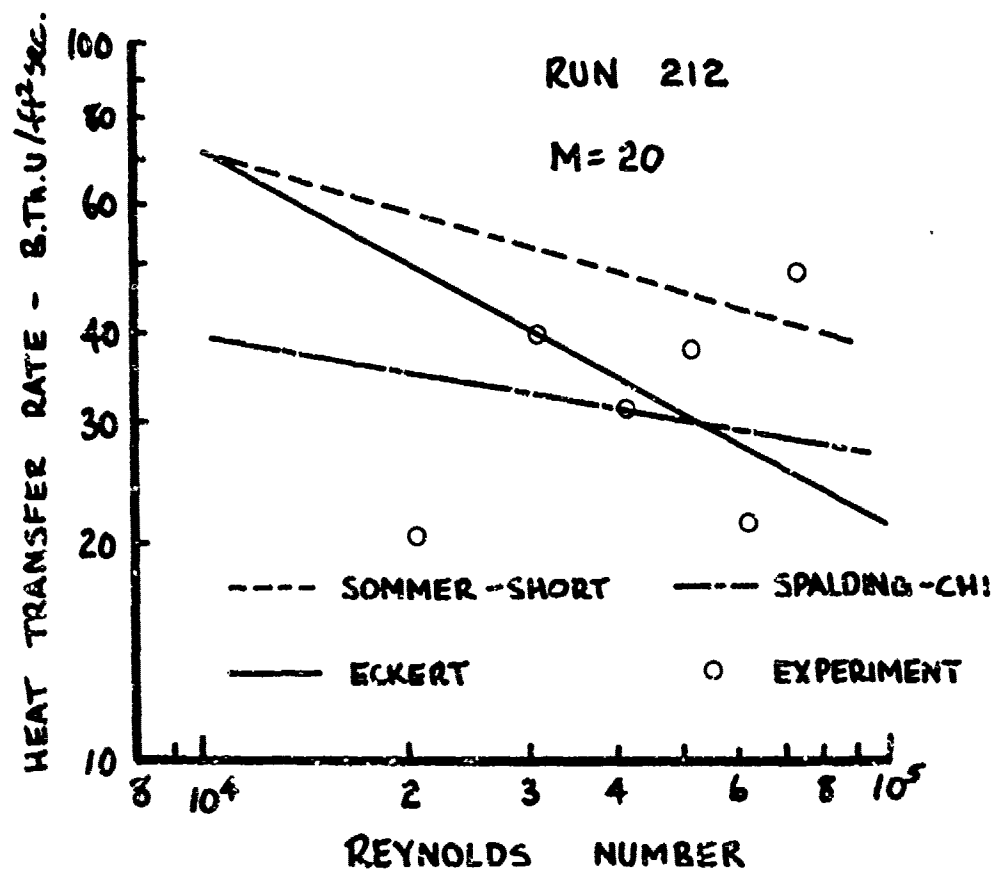


FIG. 19 HEAT TRANSFER ON ROUGH MODEL B

ω FIRST LOW RE CASE

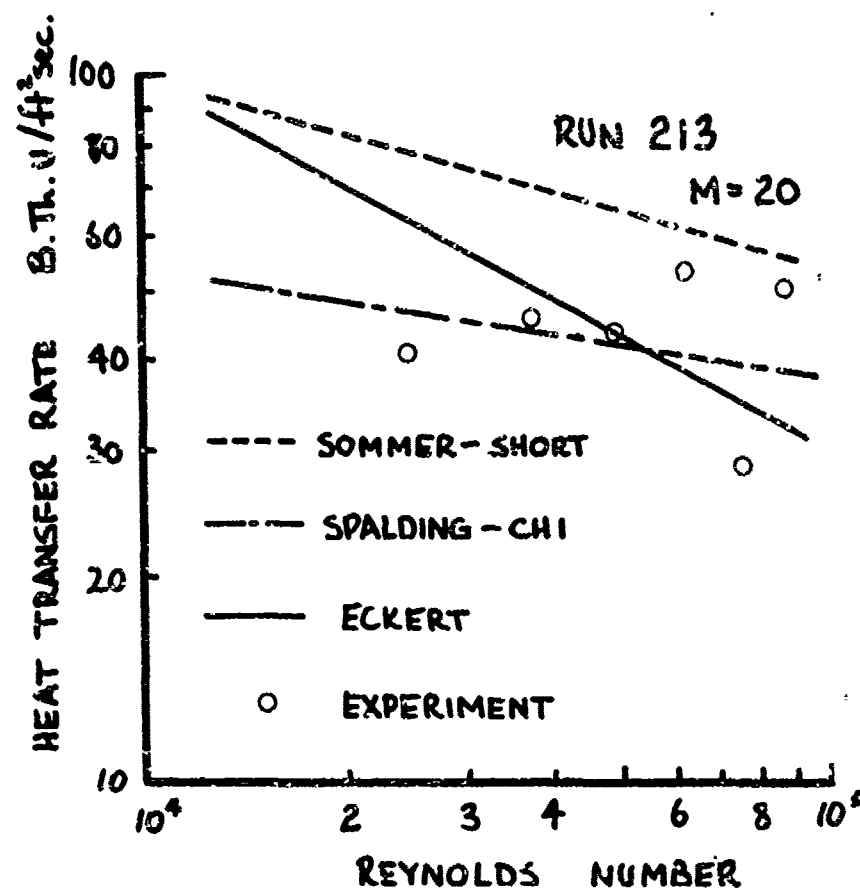


FIG. 19(Cont) HEAT TRANSFER ON ROUGH MODEL B

b) 2<sup>nd</sup> LOW RE CASE



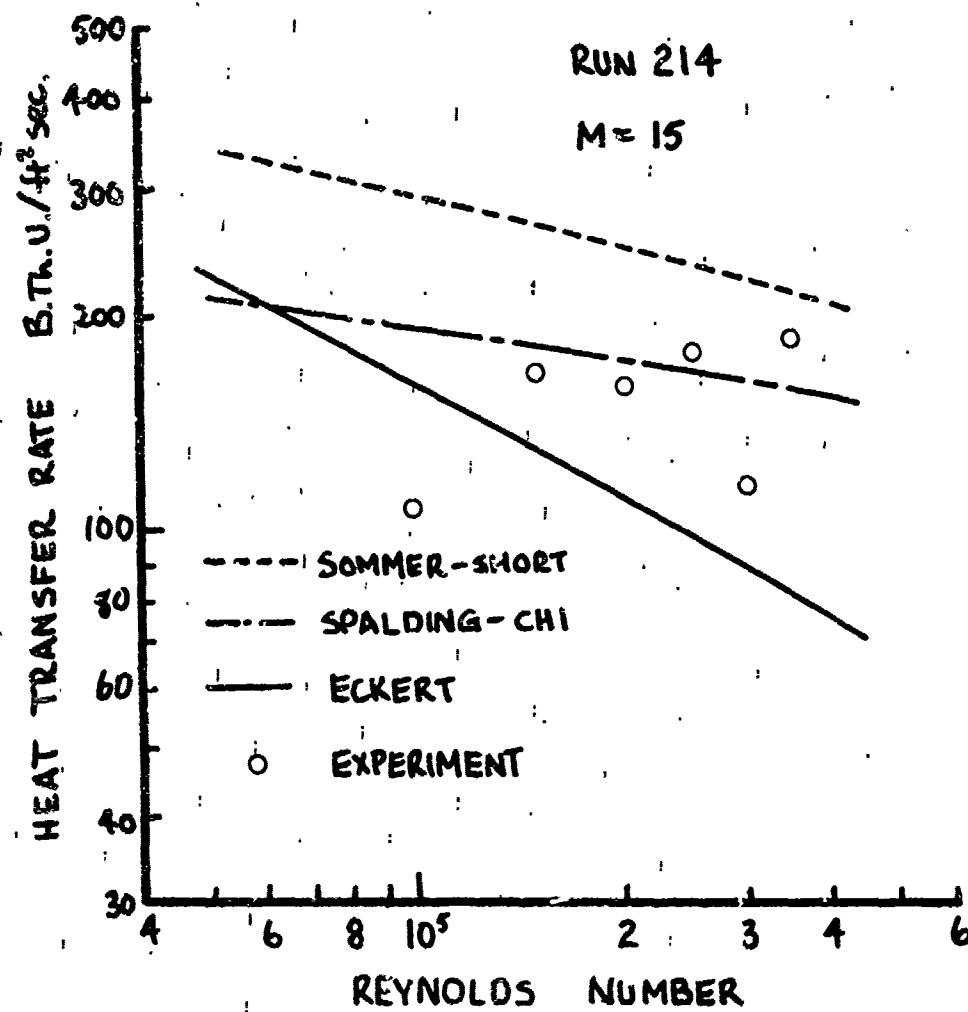


FIG. 20 HEAT TRANSFER ON ROUGH MODEL B  
M = 15

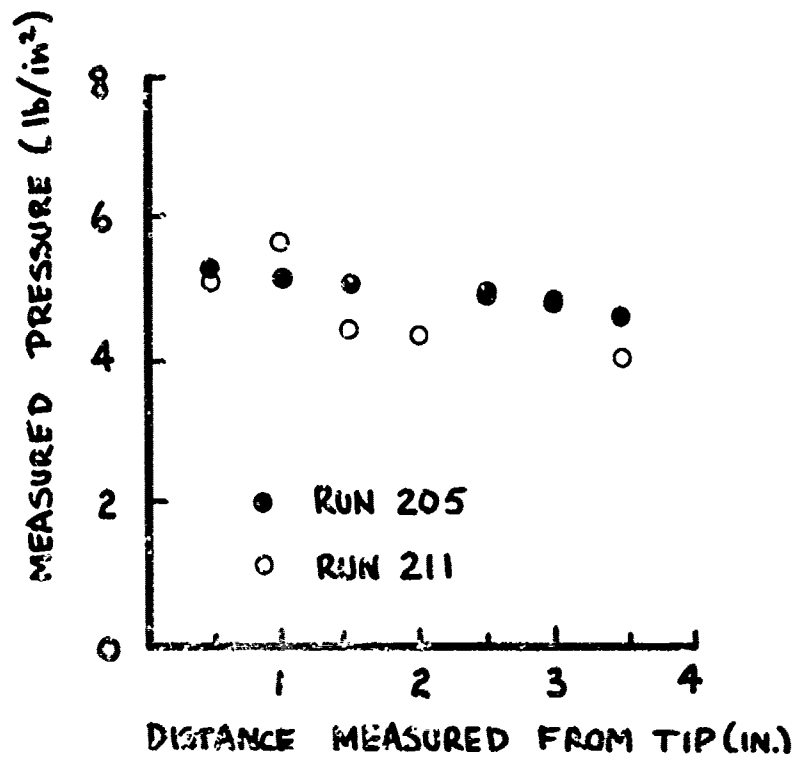


FIG. 21 PRESSURE DISTRIBUTION ON ROUGH  
MODEL B.

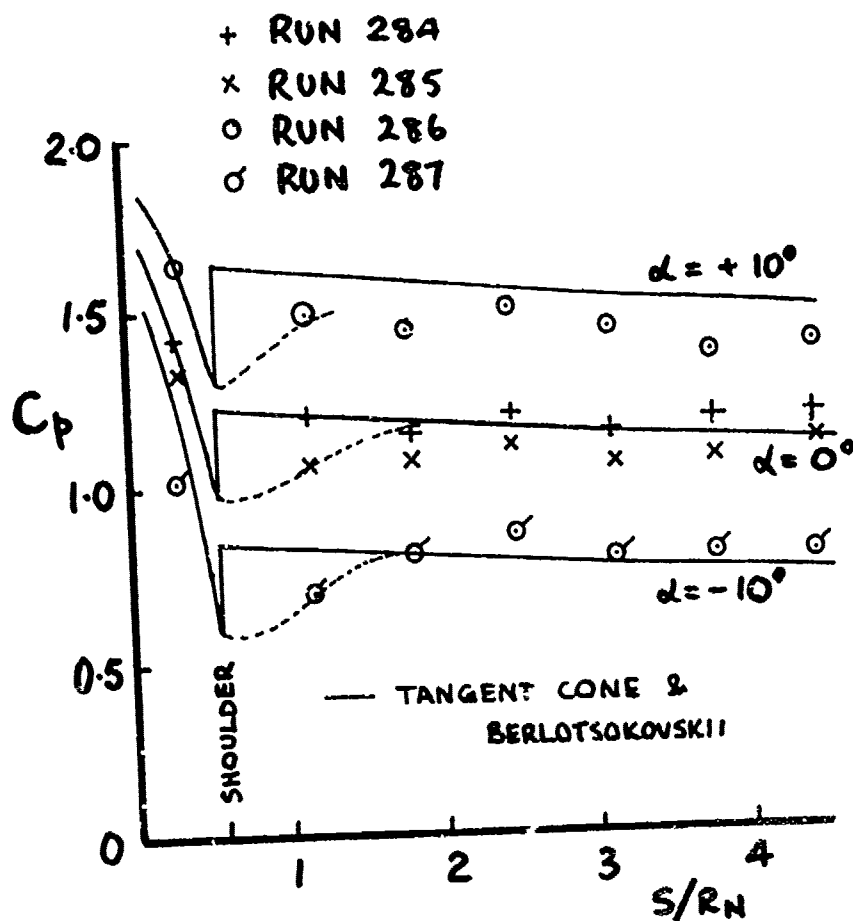
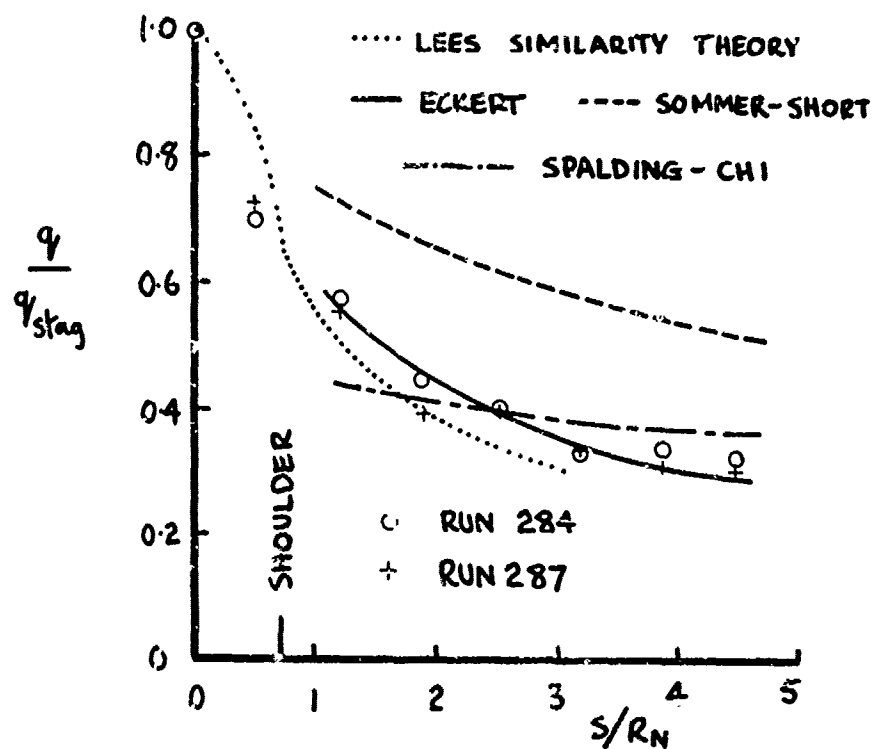
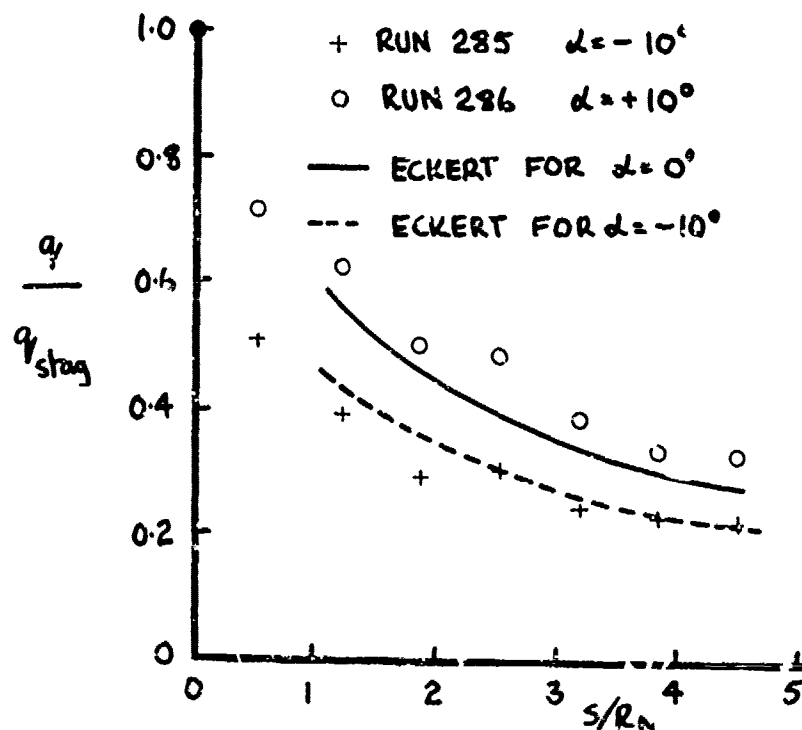


FIG 22 PRESSURE DISTRIBUTION ON  
MODEL C,  $M=20$ .

FIG. 23 HEAT TRANSFER RATE ON MODEL C AT  $\alpha = 0^\circ$ FIG. 24 HEAT TRANSFER RATE ON MODEL C AT  $\alpha = -10^\circ$  to  $+10^\circ$

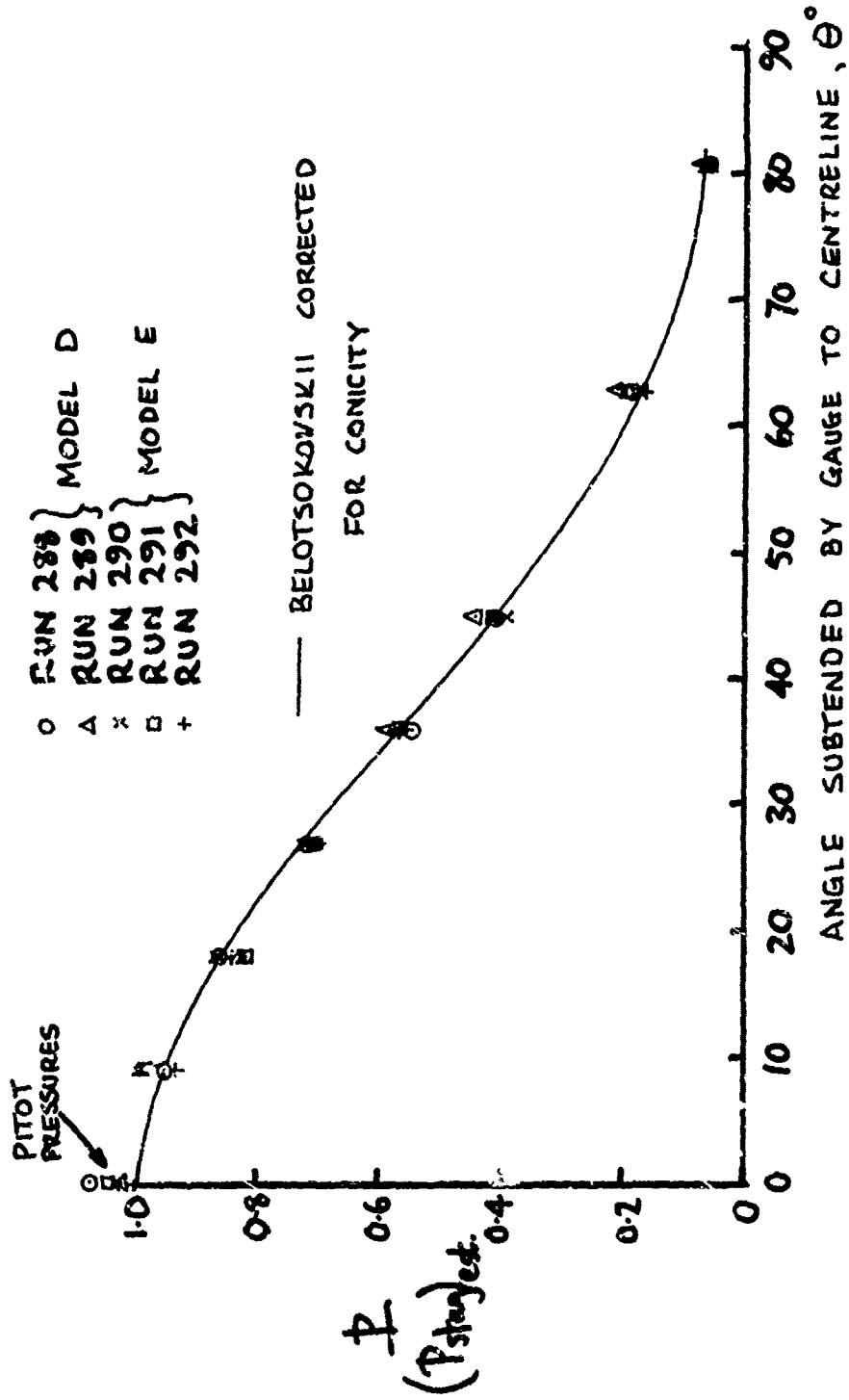


FIG 25 PRESSURE DISTRIBUTION ON MODELS D & E

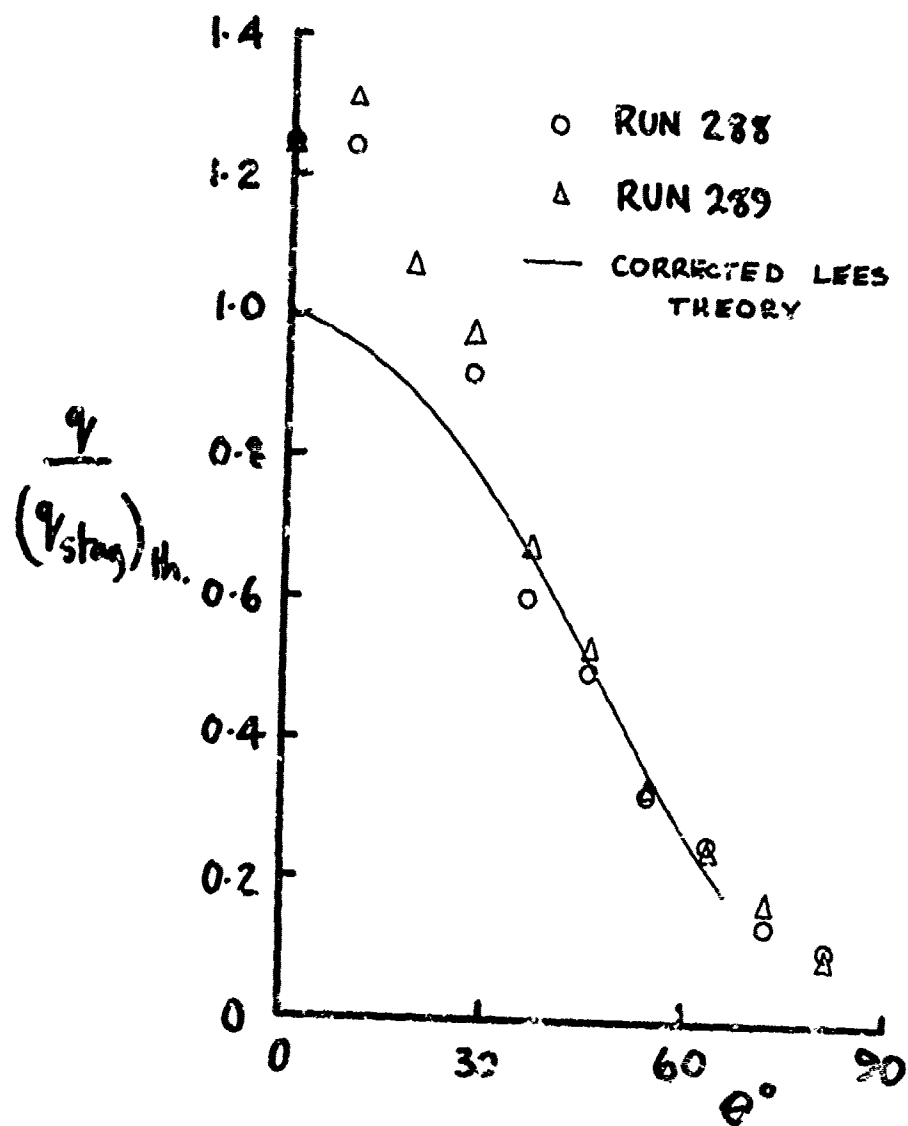


FIG 26 HEAT TRANSFER DISTRIBUTION  
ON MODEL D

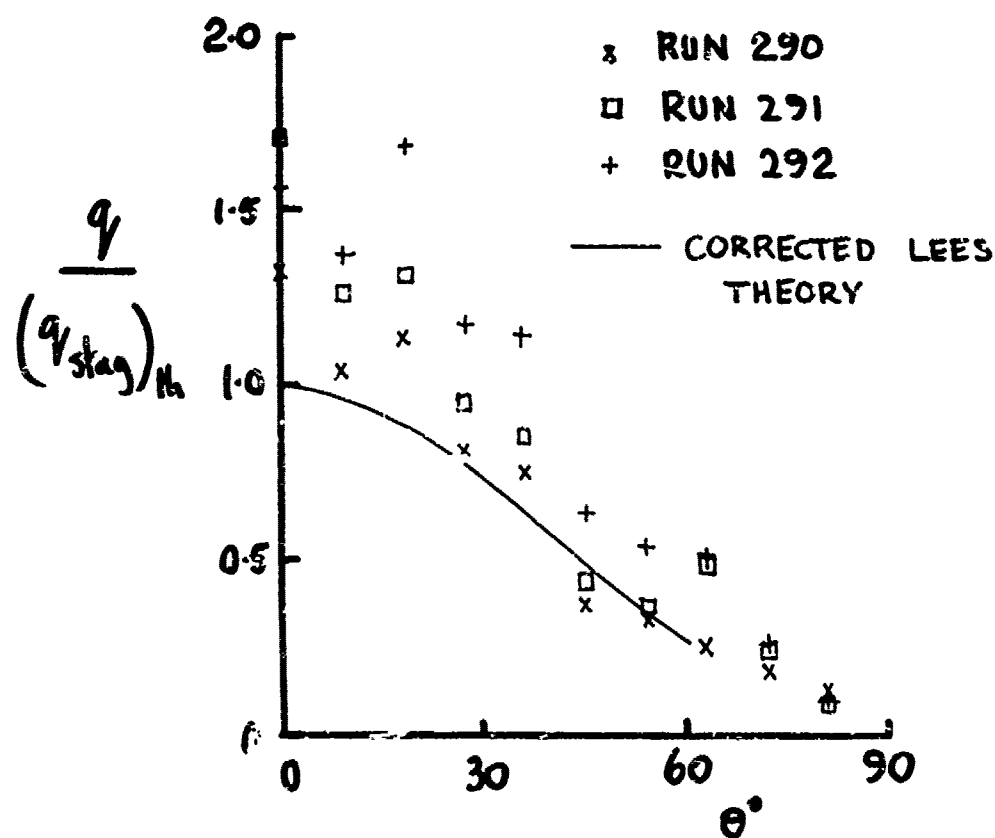


FIG 27 HEAT TRANSFER DISTRIBUTION  
O: MODEL E

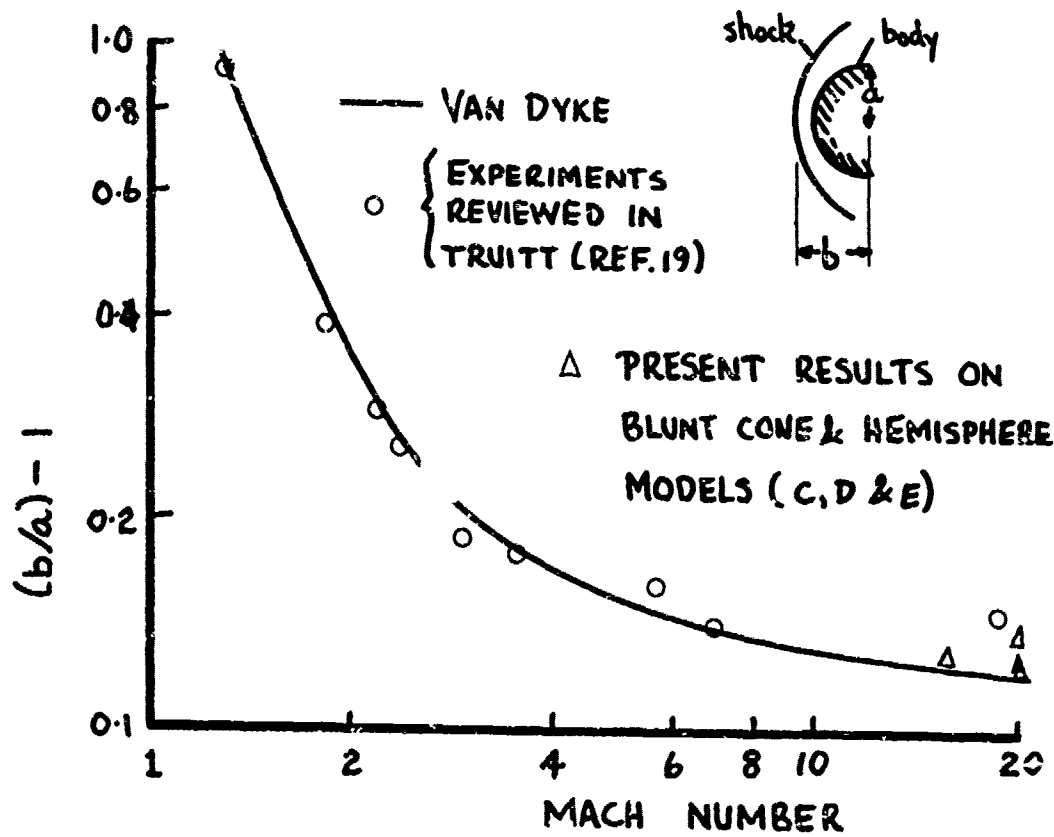
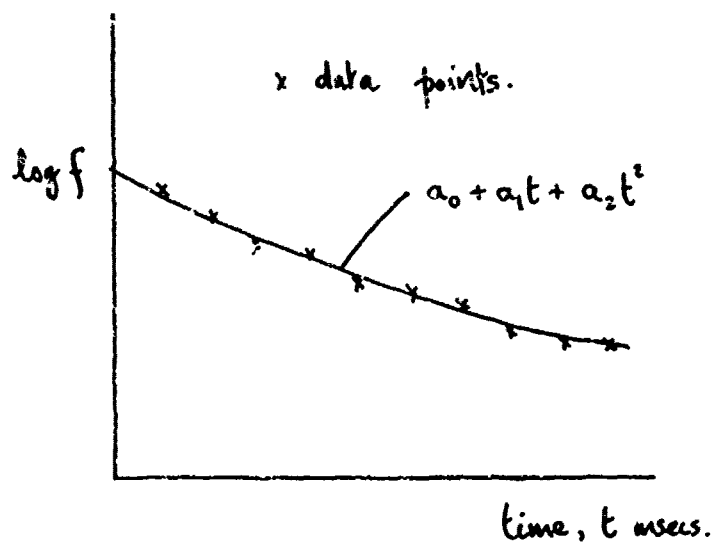


FIG. 28 SHOCK STAND-OFF DISTANCE





$$f = \exp(a_0 + a_1 t + a_2 t^2)$$

$f$  can be  $P_0$ ,  $P_{t_2}$ ,  $P$ ,  $q$  etc.

FIG. A1 CURVE FITTING PROCEDURE FOR FAST RESPONSE GAUGES.

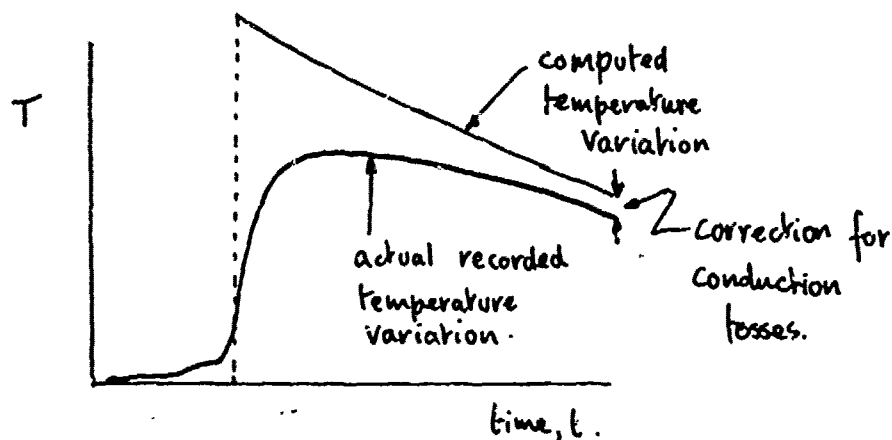


FIG. A2 METHOD OF DETERMINING TEMPERATURE VARIATION IN NOZZLE FROM A THERMOCOUPLE TRACE